

A Reduced Complexity Ungerboeck Receiver for Quantized Wideband Massive SC-MIMO

A. Bulut Üçüncü, *Student Member, IEEE*, Gökhan M. Güvensen, *Member, IEEE*,
and A. Özgür Yılmaz, *Member, IEEE*

Abstract

Employing low resolution analog-to-digital converters in massive multiple-input multiple-output (MIMO) has many advantages in terms of total power consumption, cost and feasibility of such systems. However, such advantages come together with significant challenges in channel estimation and data detection due to the severe quantization noise present. In this study, we propose a novel iterative receiver for quantized uplink single carrier MIMO (SC-MIMO) utilizing an efficient message passing algorithm based on the Busgang decomposition and Ungerboeck factorization, which avoids the use of a complex whitening filter. A reduced state sequence estimator with bidirectional decision feedback is also derived, achieving remarkable complexity reduction compared to the existing receivers for quantized SC-MIMO in the literature, without any requirement on the sparsity of the transmission channel. Moreover, the linear minimum mean-square-error (LMMSE) channel estimator for SC-MIMO under frequency-selective channel, which do not require any cyclic-prefix overhead, is also derived. We observe that the proposed receiver has significant performance gains with respect to the existing receivers in the literature under imperfect channel state information.

Index Terms

Single-carrier, analog-to-digital converter, interferer, massive MIMO, quantization, one-bit, low-resolution, uplink, Ungerboeck, Busgang decomposition, iterative.

I. INTRODUCTION

Massive multiple-input multiple-output (MIMO) systems have been enjoying considerable attention to be deployed in modern communication systems due to the many advantages they

The work of A. B. Üçüncü was supported by the ASELSAN Graduate Scholarship for Turkish Academicians.

A. B. Üçüncü, G. M. Güvensen and A. Ö. Yılmaz are with the Department of Electrical and Electronics Engineering, Middle East Technical University, 06800, Ankara, Turkey, (e-mail: {ucuncu, guvensen, aoyilmaz}@metu.edu.tr)

provide regarding spectral and energy efficiency [1]–[5]. Despite their advantages, owing to the large number of antennas, power consumption and cost of the components per antenna becomes a hindrance. Regarding this bottleneck, utilization of low-resolution analog-to-digital converters (ADCs) at each antenna of the MIMO array shines out as a feasible solution, due to their lower power consumption and cost [6]–[8]. Therefore, their utilization in massive MIMO systems have been examined intensively [8]–[17]. However, the aforementioned advantages of low resolution ADCs are not for free; there is an increased difficulty for two major tasks in such systems, namely the channel estimation and data detection, due to quantization distortion. There are many studies in the literature that handles these two important problems. In this work, we propose a novel data detector and a channel estimator for quantized wideband single-carrier (SC) massive uplink MIMO and achieve significant advantages compared to the existing work in the literature.

A. Related Work

Regarding channel estimation algorithms in quantized MIMO, there are numerous works [8], [12]–[40]. Among those studies [8], [12]–[31] propose channel estimation algorithms for flat fading channels. As quantization is a non-linear operation, the extension of flat fading channel estimation techniques to frequency-selective channels is not straightforward.

There are also many works that propose various channel estimation algorithms for frequency-selective channels in quantized MIMO systems [32]–[40]. Among them, [32] proposes a channel estimation method to estimate sparse frequency-selective channels for orthogonal frequency division multiplexing (OFDM) modulation. Another study [33] combines the expectation-maximization (EM) algorithm with a channel estimation method relying on the sparsity in the channel. However, the complexity of the algorithm in [33] can be high as it involves the maximization of M non-linear, non-convex functions over KL complex variables, M being the number of antennas, K and L being the number of users and channel taps. Due to the non-convex nature of the channel estimation problem, the global optimum solution is also not guaranteed.

More recently, [34] proposed a linear low-complexity channel estimation technique for frequency-selective channels in for MIMO-OFDM, without any sparsity assumption on the channel, where the quantization noise is assumed to be an independent identically distributed noise. This assumption is only accurate as the number of taps or users becomes large. In contrast, [35] takes into account the correlation between the quantization noise terms by deriving the linear minimum mean-square-error (LMMSE) channel estimate. Another study [36] proposes a low complexity

channel estimation algorithm based on approximate message-passing, showing some performance improvement compared to LMMSE channel estimation. However, the aforementioned channel estimation techniques [34]–[36] require OFDM and a cyclic-prefix (CP), which may decrease the spectral efficiency significantly, especially if L is large. The same OFDM or CP limitation also exists for the channel estimation techniques in [36]–[41]. In short, for all of the aforementioned channel estimation methods for frequency-selective fading, at least one of the following limitations holds: the requirement of OFDM or a CP [32], [34]–[40], the requirement of a sparse channel [32], [37]–[40], or being computationally very complex [33].

For the channel estimation algorithm to be proposed in our study, we concentrate on a linear and low complexity method in quantized massive MIMO systems under frequency selective fading, which does not require any CP and can work with single-carrier (SC) modulation. The reason for the selection of SC modulation is owing to the fact that SC is superior to OFDM for systems having nonlinearities, such as quantized MIMO [40], [42], owing to its lower peak-to-average power ratio (PAPR) [43] and robustness to carrier-frequency-offset (CFO) errors [44].

Regarding data detection in quantized massive MIMO, there are also a vast number of studies in the literature [16], [41], [42], [45]–[70]. Among them, [16], [45]–[59] propose detectors for frequency-flat channels. However, for wideband transmission, frequency-flat channel assumption is not practical, even with mmWave channels [71].

For frequency-selective channels, [41], [42], [60]–[70] advocate various data detectors for quantized massive MIMO systems. Among those work, [60] proposes a maximum *a posteriori* (MAP) data detection algorithm for quantized uplink massive MIMO-OFDM. The complexity of the proposed MAP algorithm is very high, thus suboptimal but lower complexity versions are also proposed in [60]. However, their performance is shown to be even worse than a relatively much lower complexity per subcarrier LMMSE data equalization method [68]. Another study [61] employs a generalized approximate message passing (GAMP) based detector to obtain the Bayes-optimal data estimates for quantized MIMO. However, if OFDM is not employed, the proposed detector requires the inversion of $N_c \times N_c$ matrices, N_c being the number of subcarriers, which means a complexity growth with N_c^3 , while the complexity of the detector proposed in our work grows linearly with N_c . Even with OFDM, its complexity grows with $M^2 N_c$ [61], which indicates a computationally exhaustive detector. A much recent study [41] also proposes a support vector machine based detector for one-bit massive MIMO systems, which is again limited to OFDM, requiring a CP. Moreover, the complexity of the data detection in [41] grows

with $N_c^2 K^2$ for frequency selective channels.

Owing to the aforementioned advantages of SC systems over OFDM, there are many studies proposing SC frequency domain equalization (SC-FDE) detectors in quantized MIMO. To start with, [62] proposes a GAMP based detector. However, as the proposed algorithm cannot be applied to arbitrary constellations, [62] is later extended to work with arbitrary constellations in [42] and [63]. However, the number of nonlinear operations per iteration of the proposed receivers in [42] and [63] is $5MN_cO + PKN_c$, where O is a number between 80 and 100, and P is the modulation order. As the number of antennas M in massive MIMO is large, $5MN_cO$ becomes a very large number. Moreover, the number of iterations for GAMP based methods to converge is typically about 10 iterations [61]. This means a prohibitive complexity for the detectors proposed in [42] and [63] for massive MIMO. Moreover, [64] also advocates a GAMP based receiver, but its complexity grows with N_c^2 , which can also be very high. Another SC-FDE and GAMP based detector is proposed in [65]. Nevertheless, the detector in [65] is limited to spatial modulation, which is not a commonly used modulation technique. More recently, [66] proposed various iterative detectors with feasible complexity for quantized massive MIMO.

Despite being superior compared to OFDM for quantized MIMO, there is still a CP overhead in SC-FDE. Therefore, some recent work has proposed detectors that can work without a CP for quantized SC-MIMO systems under frequency-selective fading. A sphere decoding based detector is proposed in [67] for one-bit massive MIMO. However, N being the data packet length, the complexity of the detector in [67] increases with MN^3KP for frequency-selective fading case, which is computationally infeasible. Moreover, [68] proposes a reinforcement learning based data detector. Nonetheless, the computational complexity of the detector in [68] grows with P^L [72], L being the number of channel taps. Therefore, the detector in [68] is only feasible for extremely sparse channels. In contrast, the computational complexity grows linearly with L for the proposed data detector in our work. Another detector is also proposed in [69] as a frequency domain equalizer. However, the complexity of the detector in [69] grows with NK^3 , while the proposed detector in this work has a complexity growth with NK^2 . More recently, a maximum-likelihood sequence estimator for one-bit massive MIMO under frequency-selective fading is proposed in [70]. The computational complexity of the detector in [70] grows with P^L , resulting in excessive complexity when L is large. In the same study, the necessity of a decision feedback equalization based reduced state detector is also mentioned as a future work, which is one of the important properties of the proposed detector in our work.

B. Contributions

In this study, we propose a novel iterative detector for quantized SC uplink MIMO, which will be referred to as QA-UMPA-BDF, standing for quantization-aware Ungerboeck type message passing algorithm with bidirectional decision feedback. To incorporate the quantization effects on the observation model we utilize Bussgang decomposition. An efficient message passing structure is proposed based on Ungerboeck factorization, through which we also avoid the need to use a complex noise whitening filter [73]. To further reduce the computational complexity, a reduced state sequence estimator with bidirectional decision feedback is also derived. To sum up, the main contribution items associated with our paper are as follows:

- The proposed detector is one of the few detectors in the literature that are able to work without any CP extension in quantized SC massive MIMO, which can be important to maintain a feasible spectral efficiency. In the literature, the nonlinear detectors working without CP has a complexity growth with P^L , whereas the complexity of the proposed detector grows linearly with L .
- The proposed detector is derived not only for one-bit ADCs but also for multi-bit ADCs.
- The proposed detector provides significant error-rate performance advantages over the higher complexity representative detector [66] from the literature, which even has lower spectral efficiency due to the lack of CP in our detection scheme.
- LMMSE channel estimates for CP-free SC quantized MIMO is derived based on Bussgang decomposition, which does not exist in the literature up to the knowledge of the authors.

As the benchmark detector to compare with the proposed detector, we prefer the detectors designed for SC modulation to OFDM based detectors, as SC modulation is superior to OFDM when a non-linearity is present, due to its lower PAPR [43] and robustness to CFO errors [44]. Among the aforementioned SC detectors, the ones that have comparable complexity to our detector, when the number of channel taps are not very low (if the channel is not extremely sparse), are [69] and [66]. We prefer [66] over [69] as the benchmark algorithm even if [66] has a CP overhead, since [66] is a much more recent study and the performance of [69] may be inferior to [66] due to the inter-carrier interference caused by the lack of CP in [69].

Notation: c is a scalar, \mathbf{c} is a column vector, \mathbf{C} is a matrix and \mathbf{C}^H , \mathbf{C}^T , and \mathbf{C}^* represent the Hermitian, transpose, and conjugate of matrix \mathbf{C} , respectively. $[\mathbf{C}]_{(m,n)}$ stands for the element of matrix \mathbf{C} at its m^{th} row and n^{th} column and $|\mathcal{G}|$ represents the cardinality of the set \mathcal{G} .

$\mathbb{E}[\cdot]$ takes the expectation of its operand. $\text{Re}(\cdot)$ and $\text{Im}(\cdot)$ take the real and imaginary parts of their operands and $j = \sqrt{-1}$. $\|\cdot\|$ corresponds to the Euclidean norm. $\mathbf{0}_K$ and \mathbf{I}_K are zero and identity matrices with size $K \times K$; and $\text{diag}(\mathbf{C})$ is the diagonal matrix, whose diagonal entries are equal to the diagonal entries of \mathbf{C} . Moreover, $\log_2(\cdot)$ is the base-2 logarithm, \otimes is the Kronecker product and $\text{Tr}[\cdot]$ is the trace operator. Furthermore, $\mathcal{Q}(\cdot)$ is the Q-function, which satisfies $\mathcal{Q}(x) = \frac{1}{\sqrt{2\pi}} \int_x^\infty e^{-z^2/2} dz$. The notation $\text{blkToeplitz}(\mathbf{C}, \mathbf{R})$ indicates a block Toeplitz matrix of dimension $M \times K$, whose first row block is matrix \mathbf{R} of size $M_r \times K$ and the first column block is matrix \mathbf{C} of size $M \times K_c$.

II. SYSTEM MODEL

In this study, a single-cell uplink massive MIMO system with K single-antenna users and M receive antennas equipped with low-resolution ADCs is examined. The channel between the users and the receive antennas is considered to be a frequency-selective channel. In this case, the unquantized received signal at the m^{th} antenna, namely $y_m[n]$, can be expressed as follows:

$$y_m[n] = \sum_{k=1}^K \sum_{\ell=0}^{L-1} \sqrt{\rho_k[\ell]} h_{m,k}[\ell] x_k[n - \ell] + w_m[n], \quad (1)$$

where L is the number of channel taps, $h_{m,k}[\ell]$ is the ℓ^{th} tap in the impulse response of the channel between the k^{th} user and the m^{th} receive antenna, $w_m[n]$ is the thermal noise sample received from the m^{th} antenna at the n^{th} time sample. Moreover, $\rho_k[\ell]$ is the power-delay profile of the channel between the receive antennas and the k^{th} user, satisfying $\sum_{\ell=1}^L \rho_k[\ell] = 1, \forall k$. The channel taps $h_{m,k}[\ell]$ are assumed to be zero-mean unit variance complex Gaussian random variables, corresponding to a Rayleigh fading scenario, and uncorrelated, that is, $\mathbb{E}[h_{m_1,k_1}[\ell_1] h_{m_2,k_2}[\ell_2]^*] = \delta[\ell_1 - \ell_2] \delta[k_1 - k_2] \delta[m_1 - m_2]$. Such assumptions for the channel coefficients are commonly adopted in many studies [34], [74], [75], among others. Thermal noise samples are assumed to be independent identically distributed (i.i.d) zero-mean complex Gaussian random variables with variance N_o . Moreover, $x_k[n]$ is the transmitted symbol by user k at the n^{th} time index, with average symbol energy $E_s = \mathbb{E}[|x_k[n]|^2], \forall k, n$. (1) can be more compactly written as

$$\mathbf{y}[n] = \sum_{\ell=0}^{L-1} \mathbf{H}[\ell] \mathbf{J}[\ell] \mathbf{x}[n - \ell] + \mathbf{w}[n], \quad (2)$$

where $\mathbf{J}[\ell]$ is a $K \times K$ diagonal matrix, whose k^{th} diagonal is $\sqrt{\rho_k[\ell]}$, and $\mathbf{H}[\ell]$ is the MIMO channel matrix, whose element at the m^{th} row and the k^{th} column is equal to $h_{m,k}[\ell]$. Moreover,

$\mathbf{x}[n]$ and $\mathbf{w}[n]$ are the transmitted symbol and noise vectors, whose k^{th} and m^{th} elements are equal to $x_k[n]$ and $w_m[n]$, respectively. The quantized received signal can be expressed as

$$\mathbf{r}[n] = \mathbf{Q}(\mathbf{y}[n]), \quad (3)$$

where $\mathbf{Q}(\cdot)$ is the function mapping the input of the quantizer to its output. For the case of 1-bit quantizer, $\mathbf{Q}(\cdot) = \text{sign}(\text{Re}(\cdot)) + j\text{sign}(\text{Im}(\cdot))$, $\text{sign}(\cdot)$ being the sign function.

III. LMMSE CHANNEL ESTIMATION FOR CP-FREE QUANTIZED SC-MIMO

In this section, the expression for the LMMSE channel estimate for quantized SC-MIMO systems will be derived. In the channel estimation phase, we assume that each user transmits pilot signals simultaneously. In this case, the received signal in (2) can be reexpressed as

$$\underline{\mathbf{y}}^{(p)} = (\mathbf{X} \otimes \mathbf{I}_M) \underline{\mathbf{h}} + \underline{\mathbf{w}}, \quad (4)$$

$$\underline{\mathbf{y}}^{(p)} \triangleq [\mathbf{y}[0]^T \mathbf{y}[1]^T \cdots \mathbf{y}[\tau - 1]^T]^T, \quad \underline{\mathbf{w}} \triangleq [\mathbf{w}[0]^T \mathbf{w}[1]^T \cdots \mathbf{w}[\tau - 1]^T]^T, \quad \mathbf{X} \triangleq [\mathbf{X}_1 \mathbf{X}_2 \cdots \mathbf{X}_K],$$

$$\underline{\mathbf{h}} \triangleq [(\mathbf{h}^{(1)})^T (\mathbf{h}^{(2)})^T \cdots (\mathbf{h}^{(K)})^T]^T, \quad \mathbf{h}^{(k)} \triangleq [(\mathbf{h}^{(k)}[0])^T (\mathbf{h}^{(k)}[1])^T \cdots (\mathbf{h}^{(k)}[L - 1])^T]^T,$$

in which $\mathbf{h}^{(k)}[\ell]$ is the k^{th} column of $\mathbf{H}[\ell]$ and $[\mathbf{X}_k]_{(m,n)} \triangleq \sqrt{\rho_k[n]} x_k[m - n]$. Here, τ is the training length and $x_k[n]$, $n = 0, 1, \dots, \tau - 1$ is the transmitted pilot sequence of user k .

A. Bussgang Decomposition based LMMSE Channel Estimator

To obtain a linear channel estimator having a simple expression, we utilize the Bussgang decomposition [76] which enables finding a statistically equivalent linear operator for any nonlinear function [77]. According to the Bussgang decomposition, $\underline{\mathbf{r}}^{(p)} = \mathbf{Q}(\underline{\mathbf{y}}^{(p)})$ can be written as

$$\underline{\mathbf{r}}^{(p)} = \underline{\mathbf{A}}^{(p)} \underline{\mathbf{y}}^{(p)} + \underline{\mathbf{q}}^{(p)}. \quad (5)$$

We denote the cross-covariance matrix between $\underline{\mathbf{y}}^{(p)}$ and $\underline{\mathbf{r}}^{(p)}$ by $\mathbf{C}_{\underline{\mathbf{y}}^{(p)} \underline{\mathbf{r}}^{(p)}}$ and the autocovariance matrix of $\underline{\mathbf{y}}^{(p)}$ by $\mathbf{C}_{\underline{\mathbf{y}}^{(p)}}$. When $\underline{\mathbf{A}}^{(p)}$ is selected as $\underline{\mathbf{A}}^{(p)} = \mathbf{C}_{\underline{\mathbf{y}}^{(p)} \underline{\mathbf{r}}^{(p)}}^H \mathbf{C}_{\underline{\mathbf{y}}^{(p)}}^{-1}$, the distortion term $\underline{\mathbf{q}}^{(p)}$ is minimized, or equivalently, $\underline{\mathbf{q}}^{(p)}$ is made uncorrelated with $\underline{\mathbf{y}}^{(p)}$. For a one-bit quantizer, assuming zero-mean Gaussian inputs¹, the following holds [5]:

$$\underline{\mathbf{A}}^{(p)} = \sqrt{\frac{4}{\pi}} \text{diag}(\mathbf{C}_{\underline{\mathbf{y}}^{(p)}})^{-0.5} = \sqrt{\frac{4}{\pi}} \text{diag}((\mathbf{X}\mathbf{X}^H \otimes \mathbf{I}_M) + N_o \mathbf{I}_{M\tau})^{-0.5}. \quad (6)$$

¹This assumption is approximately true even when the transmitted symbols are not Gaussian but from a finite cardinality set. The input of the ADC at the m^{th} antenna can be written as a sum of KL independent identically distributed (i.i.d.) random variables with finite variance. Owing to the central limit theorem (CLT), the value of this sum (ADC input) converge to Gaussian as KL grows large.

Equivalently, $\underline{\mathbf{A}}^{(p)}$ can be expressed as follows:

$$\underline{\mathbf{A}}^{(p)} = \mathbf{B} \otimes \mathbf{I}_M, \quad (7)$$

where $\mathbf{B} = \sqrt{4/\pi} \text{diag}(\mathbf{X}\mathbf{X}^H + N_o\mathbf{I}_\tau)^{-0.5}$. Moreover, the auto-covariance matrix of the distortion term at the quantizer output $\underline{\mathbf{q}}^{(p)}$, namely $\mathbf{C}_{\underline{\mathbf{q}}^{(p)}}$, can be found for 1-bit quantizer as [5]:

$$\mathbf{C}_{\underline{\mathbf{q}}^{(p)}} = \mathbf{C}_{\underline{\mathbf{r}}^{(p)}} - \underline{\mathbf{A}}^{(p)} \mathbf{C}_{\underline{\mathbf{y}}^{(p)}} \left(\underline{\mathbf{A}}^{(p)} \right)^H, \quad (8)$$

where $\mathbf{C}_{\underline{\mathbf{r}}^{(p)}}$ is the autocovariance matrix of $\underline{\mathbf{r}}^{(p)}$, which can be found with *arcsine law* [78]:

$$\mathbf{C}_{\underline{\mathbf{r}}^{(p)}} = \frac{4}{\pi} \left(\text{asin} \left(\mathbf{D}_{\underline{\mathbf{y}}^{(p)}}^{-\frac{1}{2}} \text{Re}(\mathbf{C}_{\underline{\mathbf{y}}^{(p)}}) \mathbf{D}_{\underline{\mathbf{y}}^{(p)}}^{-\frac{1}{2}} \right) + j \text{asin} \left(\mathbf{D}_{\underline{\mathbf{y}}^{(p)}}^{-\frac{1}{2}} \text{Im}(\mathbf{C}_{\underline{\mathbf{y}}^{(p)}}) \mathbf{D}_{\underline{\mathbf{y}}^{(p)}}^{-\frac{1}{2}} \right) \right), \quad (9)$$

where $\mathbf{D}_{\underline{\mathbf{y}}^{(p)}} = \text{diag} \left(\mathbf{C}_{\underline{\mathbf{y}}^{(p)}} \right)$. Plugging $\mathbf{C}_{\underline{\mathbf{y}}^{(p)}} = (\mathbf{X}\mathbf{X}^H \otimes \mathbf{I}_M) + N_o\mathbf{I}_{M\tau} = (\mathbf{X}\mathbf{X}^H + N_o\mathbf{I}_\tau) \otimes \mathbf{I}_M$ in (9), one can find that

$$\mathbf{C}_{\underline{\mathbf{r}}^{(p)}} = \mathbf{C}_\eta \otimes \mathbf{I}_M, \quad (10)$$

$$\mathbf{C}_\eta = \frac{4}{\pi} \left(\text{asin} \left(\mathbf{K}_{\underline{\mathbf{y}}^{(p)}}^{-\frac{1}{2}} \text{Re}(\mathbf{G}_{\underline{\mathbf{y}}^{(p)}}) \mathbf{K}_{\underline{\mathbf{y}}^{(p)}}^{-\frac{1}{2}} \right) + j \text{asin} \left(\mathbf{K}_{\underline{\mathbf{y}}^{(p)}}^{-\frac{1}{2}} \text{Im}(\mathbf{G}_{\underline{\mathbf{y}}^{(p)}}) \mathbf{K}_{\underline{\mathbf{y}}^{(p)}}^{-\frac{1}{2}} \right) \right), \quad (11)$$

$\mathbf{G}_{\underline{\mathbf{y}}^{(p)}} = (\mathbf{X}\mathbf{X}^H + N_o\mathbf{I}_\tau)$, $\mathbf{K}_{\underline{\mathbf{y}}^{(p)}} = \text{diag} \left(\mathbf{G}_{\underline{\mathbf{y}}^{(p)}} \right)$. Then, it follows from (6), (8) and (10) that

$$\mathbf{C}_{\underline{\mathbf{q}}^{(p)}} = \mathbf{E} \otimes \mathbf{I}_M, \quad (12)$$

where $\mathbf{E} = \mathbf{C}_\eta - \mathbf{B} (\mathbf{X}\mathbf{X}^H + N_o\mathbf{I}_\tau) \mathbf{B}^H$. Now that some simple expressions are found for $\underline{\mathbf{A}}^{(p)}$ and $\mathbf{C}_{\underline{\mathbf{q}}^{(p)}}$ in (7) and (12), the quantized signal $\underline{\mathbf{r}}^{(p)}$ can be found using (4), (5) and (7) as

$$\underline{\mathbf{r}}^{(p)} = (\mathbf{B}\mathbf{X} \otimes \mathbf{I}_M) \underline{\mathbf{h}} + (\mathbf{B} \otimes \mathbf{I}_M) \underline{\mathbf{w}} + \underline{\mathbf{q}}^{(p)}. \quad (13)$$

Let $\underline{\mathbf{\Gamma}} \triangleq (\mathbf{B} \otimes \mathbf{I}_M) \underline{\mathbf{w}} + \underline{\mathbf{q}}^{(p)}$, which corresponds to the total effective noise at the quantizer output. Its covariance matrix $\mathbf{C}_{\underline{\mathbf{\Gamma}}}$ can be found using (12) and (13) as

$$\mathbf{C}_{\underline{\mathbf{\Gamma}}} = \mathbf{F} \otimes \mathbf{I}_M, \quad (14)$$

where $\mathbf{F} = N_o\mathbf{B}\mathbf{B}^H + \mathbf{E}$. Now that, the effective noise covariance matrix is found, we can apply a whitening filter, $\mathbf{C}_{\underline{\mathbf{\Gamma}}}^{-1/2} = \mathbf{F}^{-1/2} \otimes \mathbf{I}_M$, to obtain

$$\underline{\mathbf{z}}^{(p)} \triangleq \mathbf{C}_{\underline{\mathbf{\Gamma}}}^{-1/2} \underline{\mathbf{r}}^{(p)} = (\mathbf{P}\mathbf{X} \otimes \mathbf{I}_M) \underline{\mathbf{h}} + \underline{\mathbf{n}}, \quad (15)$$

where $\mathbf{P} = \mathbf{F}^{-1/2}\mathbf{B}$ and $\underline{\mathbf{n}} = (\mathbf{P} \otimes \mathbf{I}_M) \underline{\mathbf{w}} + \mathbf{F}^{-1/2}\underline{\mathbf{q}}^{(p)}$, whose covariance matrix $\mathbf{C}_{\underline{\mathbf{n}}} = \mathbf{I}_{M\tau}$. To derive the LMMSE estimator from the whitened observations, we also need to find whether $\underline{\mathbf{h}}$ and $\underline{\mathbf{n}}$ are uncorrelated. It has been shown in [35, Appendix A] that for any quantized LMMSE channel estimation based on Bussgang decomposition, the quantization distortion term, which is

$\mathbf{q}^{(p)}$ in our work, is uncorrelated with the channel estimates, implying that \mathbf{u} is also uncorrelated with \mathbf{h} as \mathbf{w} is also uncorrelated with \mathbf{h} . In this case, $\mathbf{C}_{\mathbf{z}^{(p)}} \triangleq \mathbb{E}[\mathbf{z}^{(p)}\mathbf{z}^{(p)H}]$ can be found as

$$\mathbf{C}_{\mathbf{z}^{(p)}} = \left(\mathbf{X}'\mathbf{X}'^H \otimes \mathbf{I}_M \right) + \mathbf{I}_{M\tau}, \quad (16)$$

where $\mathbf{X}' = \mathbf{P}\mathbf{X}$. $\mathbf{C}_{\mathbf{z}^{(p)}\mathbf{h}} \triangleq \mathbb{E}[\mathbf{z}^{(p)}\mathbf{h}^H]$ can also be obtained as

$$\mathbf{C}_{\mathbf{z}^{(p)}\mathbf{h}} = (\mathbf{X}' \otimes \mathbf{I}_M). \quad (17)$$

Consequently, the LMMSE channel estimate for CP-free wideband one-bit massive MIMO, namely $\hat{\mathbf{h}}^{\text{LME}}$, can be found using (16) and (17) as

$$\hat{\mathbf{h}}^{\text{LME}} = \mathbf{C}_{\mathbf{z}^{(p)}\mathbf{h}}^H \mathbf{C}_{\mathbf{z}^{(p)}}^{-1} \mathbf{z}^{(p)} = (\mathbf{X}' \otimes \mathbf{I}_M)^H \left(\left(\mathbf{X}'\mathbf{X}'^H \otimes \mathbf{I}_M \right) + \mathbf{I}_{M\tau} \right)^{-1} \mathbf{z}^{(p)}. \quad (18)$$

Note that in (18), the inverse of a $M\tau \times M\tau$ matrix should be taken. To obtain a lower complexity LMMSE estimator, we define $\mathbf{X}'' \triangleq \mathbf{X}' \otimes \mathbf{I}_M$. Then, (18) can be rewritten as

$$\hat{\mathbf{h}}^{\text{LME}} = (\mathbf{X}' \otimes \mathbf{I}_M)^H \left(\left(\mathbf{X}'\mathbf{X}'^H \otimes \mathbf{I}_M \right) + \mathbf{I}_{M\tau} \right)^{-1} \mathbf{z}^{(p)} = \mathbf{X}''^H \left(\mathbf{X}''\mathbf{X}''^H + \mathbf{I}_{M\tau} \right)^{-1} \mathbf{z}^{(p)}. \quad (19)$$

Employing Woodbury matrix identity [79], (19) can be reexpressed as

$$\begin{aligned} \hat{\mathbf{h}}^{\text{LME}} &= \left((\mathbf{X}'')^H \mathbf{X}'' + \mathbf{I}_{MKL} \right)^{-1} (\mathbf{X}'')^H \mathbf{z}^{(p)} \\ &= \left(\left((\mathbf{X}')^H \mathbf{X}' \otimes \mathbf{I}_M \right) + \mathbf{I}_{MKL} \right)^{-1} (\mathbf{X}'')^H \mathbf{z}^{(p)} \\ &= \left((\mathbf{X}^H \mathbf{P}^H \mathbf{P} \mathbf{X} + \mathbf{I}_{KL})^{-1} \otimes \mathbf{I}_M \right) (\mathbf{P} \mathbf{X} \otimes \mathbf{I}_M)^H \mathbf{z}^{(p)}. \end{aligned} \quad (20)$$

In (20), the inverse of a $KL \times KL$ matrix is taken, which is much less complex than taking the inverse of an $M\tau \times M\tau$ matrix in (18), as $\tau \geq KL$ in general (for orthogonal pilot assignment to users $\tau \geq KL$). The complexity to calculate the proposed LMMSE channel estimate is much less than the one derived in [35] for OFDM with a CP decreasing spectral efficiency. The LMMSE expression in [35] requires the inverse of a large $M\tau \times M\tau$ matrix, as M is large in massive MIMO and $\tau \geq KL$ in general. Mean-square-error (MSE) matrix can also be calculated as

$$\mathbf{C}_{\hat{\mathbf{h}}}^{\text{LME}} = \mathbf{I}_{MKL} - \left((\mathbf{X}^H \mathbf{P}^H \mathbf{P} \mathbf{X} + \mathbf{I}_{KL})^{-1} \otimes \mathbf{I}_M \right) (\mathbf{X}^H \mathbf{P}^H \mathbf{P} \mathbf{X} \otimes \mathbf{I}_M). \quad (21)$$

B. Low Complexity Approximations for the LMMSE Estimator

In this section, we will show that an even lower complexity approximation for LMMSE channel estimate exists under some conditions. One of those conditions are when $\mathbf{X}\mathbf{X}^H$ is diagonally dominant. This happens when the pilots assigned to different users are nearly orthogonal and the

autocorrelation function of the transmitted pilot sequence of all users is close to a single impulse function, that is $\sum_{n=0}^{L-1} \sqrt{\rho_k[n]} \sqrt{\rho_{k'}[n]} x_k[m-n] x_{k'}^*[m'-n] \approx U \delta[m-m'] \delta[k-k']$, where U is an arbitrary constant. This approximation is accurate when users transmit randomly generated complex symbols as pilot sequences and KL is large. Another condition for LMMSE channel estimate to have a lower complexity approximation is the SNR being low. For both cases (for low SNR or when $\mathbf{X}\mathbf{X}^H$ is diagonally dominant) $\mathbf{C}_{\underline{\mathbf{y}}^{(p)}} = (\mathbf{X}\mathbf{X}^H \otimes \mathbf{I}_M) + N_o \mathbf{I}_{M\tau}$ is diagonally dominant, thus the following approximation, which can be written using (8)-(10), is tight:

$$\mathbf{C}_{\underline{\mathbf{q}}^{(p)}} \approx (2 - 4/\pi) \mathbf{I}_{M\tau}. \quad (22)$$

In this case, the overall effective noise becomes uncorrelated. Then, the complexity of the calculation of the whitening filter $\mathbf{C}_{\underline{\mathbf{F}}}^{-1/2} = \mathbf{F}^{-1/2} \otimes \mathbf{I}_M$ is reduced significantly as \mathbf{F} became a diagonal matrix for uncorrelated effective noise. This makes $\mathbf{P} = \mathbf{F}^{-1/2} \mathbf{B}$ a diagonal matrix as \mathbf{B} is a diagonal matrix by definition, reducing the complexity in calculating (20).

A further reduction in the complexity of the LMMSE channel estimator is possible by assuming that $\mathbf{B} = \sqrt{4/\pi} \text{diag}(\mathbf{X}\mathbf{X}^H + N_o \mathbf{I}_\tau)^{-0.5}$ is a constant diagonal matrix. This is an accurate assumption when SNR is low. Even if SNR is not low, it is valid to assume that the diagonal elements of $\mathbf{X}\mathbf{X}^H$, corresponding to the average received power for each received sample at each antenna (averaged over channel realizations), which are equal to $\sum_{\ell=0}^{L-1} \sum_{k=0}^{K-1} \rho_k[l] |x_k[m-\ell]|^2$ for all receive antennas at the m^{th} received sample, does not change over the pilot symbol transmission phase for most cases. If the magnitude of the transmitted complex pilot symbols are always the same, which is the case for DFT pilot sequences or any sequence generated randomly from a phase-shift keying (PSK) type modulation, this assumption is exactly correct. Otherwise, the approximation error caused by this assumption goes to zero as KL becomes large. With this assumption, \mathbf{B} can be approximated as

$$\mathbf{B} = \sqrt{4/\pi} \text{diag}(\mathbf{X}\mathbf{X}^H + N_o \mathbf{I}_\tau)^{-0.5} \approx g \mathbf{I}_\tau, \quad (23)$$

where $g = \sqrt{4/(\pi(K E_s + N_o))}$. Along with (22), this implies that

$$\mathbf{P} = \mathbf{F}^{(-1/2)} \mathbf{B} \approx (2 - 4/\pi + g^2 N_o)^{(-1/2)} g \mathbf{I}_\tau. \quad (24)$$

Then, the LMMSE estimator in (20) and MSE expression in (21) can be approximated as

$$\hat{\underline{\mathbf{h}}}^{\text{LME}} \approx \left((c^2 \mathbf{X}^H \mathbf{X} + \mathbf{I}_{KL})^{-1} \otimes \mathbf{I}_M \right) (c \mathbf{X} \otimes \mathbf{I}_M)^H \underline{\mathbf{z}}^{(p)}, \quad (25)$$

$$\mathbf{C}_{\hat{\underline{\mathbf{h}}}}^{\text{LME}} \approx \mathbf{I}_{MKL} - \left((c^2 \mathbf{X}^H \mathbf{X} + \mathbf{I}_{KL})^{-1} \otimes \mathbf{I}_M \right) (c^2 \mathbf{X}^H \mathbf{X} \otimes \mathbf{I}_M), \quad (26)$$

where $c = g/\sqrt{2 - 4/\pi + g^2 N_o}$. By approximating $\mathbf{X}\mathbf{X}^H$ as a constant diagonal matrix (with diagonal entries being $KE_s + N_o$), which is an accurate assumption under the conditions mentioned above, expressions of even lower complexity to calculate can be written from (19) as

$$\hat{\mathbf{h}}^{\text{LME}} \approx \frac{c(\mathbf{X} \otimes \mathbf{I}_M)^H \mathbf{z}^{(p)}}{c^2 E_s K + 1}, \mathbf{C}_{\hat{\mathbf{h}}}^{\text{LME}} \approx \left(1 - \frac{c^2 (\mathbf{X}^H \mathbf{X} \otimes \mathbf{I}_M)}{c^2 E_s K + 1}\right), \quad (27)$$

which are very simple expressions not involving any matrix inversions.

C. Extension to multi-bit quantizers

The LMMSE channel estimator and the resulting MSE expression for multi-bit quantizers are the same as (20) and (21) for 1-bit quantizer, except that the matrices \mathbf{B} and \mathbf{E} employed in the derivation of (20) and (21) are modified. For the example case of multi-bit midrise uniform quantizers with Gaussian inputs¹, \mathbf{B} in (7) can be found as [74],

$$\mathbf{B} = \frac{\Delta}{\sqrt{\pi}} \text{diag}(\mathbf{X}\mathbf{X}^H + N_o \mathbf{I}_\tau)^{-0.5} \sum_{i=1}^{2^q-1} \exp\left(-\Delta^2 (i - 2^{q-1})^2 \text{diag}(\mathbf{X}\mathbf{X}^H + N_o \mathbf{I}_\tau)^{-0.5}\right), \quad (28)$$

where Δ is the quantizer step size and q is the number of quantizer bits. Moreover, \mathbf{E} in (12) for multi-bit quantizer case can be approximated using [74]

$$\begin{aligned} \mathbf{E} \approx & \frac{\Delta^2}{2} (2^q - 1)^2 \mathbf{I}_{M\tau} - \mathbf{B} \text{diag}(\mathbf{X}\mathbf{X}^H + N_o \mathbf{I}_\tau) \mathbf{B}^H \\ & - 4\Delta^2 \sum_{i=1}^{2^q-1} (i - 2^{q-1}) \times \left(1 - \mathcal{Q}\left(\sqrt{2}(i - 2^{q-1}) \text{diag}(\mathbf{X}\mathbf{X}^H + N_o \mathbf{I}_\tau)^{-1/2}\right)\right). \end{aligned} \quad (29)$$

Moreover, for the lower complexity LMMSE channel estimator calculations in Section III-B, replacing $\mathbf{X}\mathbf{X}^H$ by a constant diagonal matrix with diagonal entries being (KE_s) , defining $P_r \triangleq KE_s + N_o$ the following approximations can be used for the multi-bit quantizer case

$$g = \sqrt{\Delta^2 / (\pi P_r)} \times \sum_{i=1}^{2^q-1} \exp\left(-\Delta^2 (i - 2^{q-1})^2 / \sqrt{(P_r)}\right), c \approx g / \sqrt{(d + g^2 N_o)}, \quad (30)$$

$$d = \frac{\Delta^2}{2} (2^q - 1)^2 - g^2 (P_r) - 4\Delta^2 \sum_{i=1}^{2^q-1} (i - 2^{q-1}) \times \left(1 - \mathcal{Q}\left(\sqrt{2}(i - 2^{q-1}) (P_r)^{-1/2}\right)\right). \quad (31)$$

IV. DATA TRANSMISSION

For the data transmission phase, the quantized received signal can be rewritten using (2) as

$$\mathbf{r}^{(d)} = \mathbf{Q}(\mathbf{y}^{(d)}) = \mathbf{Q}(\mathbf{H}\mathbf{x} + \mathbf{w}), \quad (32)$$

$$\underline{\mathbf{y}}^{(d)} \triangleq [\mathbf{y}[0]^T \ \mathbf{y}[1]^T \ \cdots \ \mathbf{y}[N+L-2]^T]^T, \quad \underline{\mathbf{w}} \triangleq [\mathbf{w}[0]^T \ \mathbf{w}[1]^T \ \cdots \ \mathbf{w}[N+L-2]^T]^T,$$

$$\underline{\mathbf{H}} \triangleq \text{blkToeplitz}(\underline{\mathbf{H}}^c, \underline{\mathbf{H}}^r), \quad \underline{\mathbf{x}} \triangleq [\mathbf{x}[0]^T \ \mathbf{x}[1]^T \ \cdots \ \mathbf{x}[N-1]^T]^T, \quad (33)$$

$\underline{\mathbf{H}}^c \triangleq \begin{bmatrix} \tilde{\mathbf{H}}[0] & \mathbf{0} & \cdots & \mathbf{0} \end{bmatrix}$ with size $M \times NK$ and $\underline{\mathbf{H}}^r \triangleq \begin{bmatrix} \tilde{\mathbf{H}}[0]^T & \tilde{\mathbf{H}}[1]^T & \cdots & \tilde{\mathbf{H}}[L-1]^T & \mathbf{0} \cdots \mathbf{0} \end{bmatrix}^T$ with size $(N+L-2)M \times K$, in which $\tilde{\mathbf{H}}[\ell] = \mathbf{H}[\ell]\mathbf{J}[\ell]$. Note that despite the same or similar notations are used for the data/pilot and noise vectors for the channel estimation and data transmission signal models for simplicity, they are completely independent of each other. Using Bussgang decomposition [76], (32) can be reexpressed as

$$\underline{\mathbf{r}}^{(d)} = \underline{\mathbf{A}}^{(d)} \underline{\mathbf{H}} \underline{\mathbf{x}} + \underline{\mathbf{A}}^{(d)} \underline{\mathbf{w}} + \underline{\mathbf{q}}^{(d)}, \quad (34)$$

where $\underline{\mathbf{A}}^{(d)}$ can be found by replacing $\mathbf{C}_{\underline{\mathbf{y}}^{(p)}}$ in (6) by $\mathbf{C}_{\underline{\mathbf{y}}^{(d)}} \triangleq \underline{\mathbf{H}}\underline{\mathbf{H}}^H + N_o\mathbf{I}_{M(N+L-2)}$ for one-bit quantizer or by replacing $\mathbf{X}\mathbf{X}^H + N_o\mathbf{I}_\tau$ in (28) by $\mathbf{C}_{\underline{\mathbf{y}}^{(d)}}$ for multi-bit uniform midrise quantizer. Moreover, the quantizer distortion term covariance matrix for one-bit quantizer case, namely $\mathbf{C}_{\underline{\mathbf{q}}^{(d)}}$, can also be found by replacing $\mathbf{C}_{\underline{\mathbf{y}}^{(p)}}$, $\mathbf{C}_{\underline{\mathbf{r}}^{(p)}}$ and $\underline{\mathbf{A}}^{(p)}$ in (8) and (9) by $\mathbf{C}_{\underline{\mathbf{y}}^{(d)}}$, $\mathbf{C}_{\underline{\mathbf{r}}^{(d)}} \triangleq \mathbb{E}[\underline{\mathbf{r}}^{(d)}\underline{\mathbf{r}}^{(d)H}]$ and $\underline{\mathbf{A}}^{(d)}$, respectively. For multi-bit quantizer case, $\mathbf{C}_{\underline{\mathbf{q}}^{(d)}}$ can also be obtained by replacing $\mathbf{X}\mathbf{X}^H + N_o\mathbf{I}_\tau$ and $\mathbf{I}_{M\tau}$ in (29) by $\mathbf{C}_{\underline{\mathbf{y}}^{(d)}}$ and $\mathbf{I}_{M(N+L-2)}$, respectively. Moreover, as the channel coefficients are taken to be i.i.d. unit variance random variables, all diagonal elements of $\underline{\mathbf{H}}\underline{\mathbf{H}}^H$ converge to KE_s as KL goes large, the reason of which is discussed previously. Moreover, when KL is large or for low SNR, again it is straightforward to show that $\underline{\mathbf{H}}\underline{\mathbf{H}}^H + N_o\mathbf{I}_{M(N+L-2)}$ is a diagonally dominant matrix with diagonal entries converging to $KE_s + N_o$. In this case (when $\underline{\mathbf{H}}\underline{\mathbf{H}}^H + N_o\mathbf{I}_{M(N+L-2)} \approx (KE_s + N_o)\mathbf{I}_{M(N+L-2)}$), $\underline{\mathbf{A}}^{(d)}$ and $\mathbf{C}_{\underline{\mathbf{q}}^{(d)}}$ can be approximated by employing the modified versions of (6), (28), (8), (9) for data transmission phase (with the aforementioned modifications such as replacing $\mathbf{C}_{\underline{\mathbf{y}}^{(p)}}$ by $\mathbf{C}_{\underline{\mathbf{y}}^{(d)}}$) as

$$\underline{\mathbf{A}}^{(d)} \approx a\mathbf{I}_{M(N+L-2)}, \quad \mathbf{C}_{\underline{\mathbf{q}}^{(d)}} \approx e\mathbf{I}_{M(N+L-2)}, \quad (35)$$

where $a = \sqrt{4/(\pi(KE_s + N_o))}$, $e = 2 - 4/\pi$ for one-bit quantizer case. For multi-bit quantizer case $a = g$, where g can be found using (30) and $e = d$, where d can be found using (31). The aforementioned assumptions, leading to an uncorrelated quantizer noise assumption, are observed to be accurate even when the number of users are as low as $K = 4$ and $L = 1$ for i.i.d. channel coefficients [35, Fig. 4], even for high SNR. In fact, K and L values will be much larger in general, implying very low approximation errors.

V. QUANTIZATION AWARE UNGERBOECK TYPE MESSAGE PASSING ALGORITHM WITH BIDIRECTIONAL DECISION FEEDBACK

Based on (34) and (35), a minimum distance performance metric can be constructed as

$$\Lambda(\underline{\mathbf{r}}, \underline{\mathbf{H}}, \underline{\mathbf{x}}) = \gamma_1 \exp(-\|\underline{\mathbf{r}} - \underline{\mathbf{H}}\underline{\mathbf{x}}\|^2), \quad (36)$$

where $\underline{\mathbf{r}} = \mathbf{r}/\sqrt{e}$, $\underline{\mathbf{H}} = a\mathbf{H}/\sqrt{e}$ and γ_1 is a multiplicative constant. The metric corresponds to the ML metric when the effective noise term $(a\underline{\mathbf{w}}) + \underline{\mathbf{q}}$ has a Gaussian distribution. It has been pointed out in [80]–[82] that the Gaussian assumption for the quantization noise $(a\underline{\mathbf{w}}) + \underline{\mathbf{q}}$ yields accurate results, especially for low SNR, even for 1-bit quantizer. As a gets closer to 1 and the power of quantizer noise $\underline{\mathbf{q}}$ decreases with increasing number of resolution bits, it can be stated that the effective noise $(a\underline{\mathbf{w}}) + \underline{\mathbf{q}}$ can be approximated as Gaussian for all quantization resolutions, as the $(a\underline{\mathbf{w}})$ term in the effective noise dominates.

We continue by rewriting the minimum distance metric in (36) as

$$\Lambda(\underline{\mathbf{r}}, \underline{\mathbf{H}}, \underline{\mathbf{x}}) = \gamma_2 \exp(2\Re(\underline{\mathbf{r}}^H \underline{\mathbf{H}} \underline{\mathbf{x}}) - \underline{\mathbf{x}}^H \underline{\mathbf{H}}^H \underline{\mathbf{H}} \underline{\mathbf{x}}). \quad (37)$$

To obtain the optimal estimates based on the metric in (37), there are various approaches. One is to filter $\underline{\mathbf{r}}$ by a channel matched filter (CMF) followed by a noise whitening filter in the Forney method [83]. The complexity of this method including a whitening filter can be high, thus an alternative method based on Ungerboeck observation model can be chosen [83]. In the Ungerboeck observation model, the minimum distance metric is constructed directly from the unwhitened CMF output, namely $\mathbf{v} \triangleq \underline{\mathbf{H}}^H \underline{\mathbf{r}}$. Taking \mathbf{v} as the observation vector, the metric in (37) can be rewritten as

$$\Lambda(\underline{\mathbf{r}}, \underline{\mathbf{H}}, \underline{\mathbf{x}}) = \gamma_2 \exp(2\Re(\mathbf{v}^H \underline{\mathbf{x}}) - \underline{\mathbf{x}}^H \mathbf{G} \underline{\mathbf{x}}), \quad (38)$$

where $\mathbf{G} \triangleq \underline{\mathbf{H}}^H \underline{\mathbf{H}} \triangleq \text{blkToeplitz}(\mathbf{G}^c, \mathbf{G}^r)$, in which $\mathbf{G}^r = [\mathbf{G}[0] \ \mathbf{G}[1] \ \cdots \ \mathbf{G}[L-1] \ \mathbf{0} \ \cdots \ \mathbf{0}]$, $\mathbf{G}^c = (\mathbf{G}^r)^H$, where $\mathbf{G}[\ell] \triangleq \frac{a^2}{e} \sum_{k=0}^{L-1-\ell} \tilde{\mathbf{H}}[k+\ell]^H \tilde{\mathbf{H}}[k]$.

With these definitions, the minimum distance metric in (38) can be computed recursively as

$$\begin{aligned} \Lambda_N &= \sum_{n=0}^{N-1} (\Lambda_{n+1} - \Lambda_n) \\ &= \sum_{n=0}^{N-1} \left(\sum_{k=1}^K \left[\kappa_k^n(v_k[n], x_k[n]) - \phi_k^n(x_k[n], \mathbf{S}_k^n) - \sum_{k'=1, k' < k}^K \psi_{k, k'}^n(x_k[n], \mathbf{S}_k^n, x_{k'}[n], \mathbf{S}_{k'}^n) \right] \right), \end{aligned} \quad (39)$$

where $\Lambda_N = \Lambda(\underline{v}, \underline{\mathbf{H}}, \underline{\mathbf{x}})$, $v_k[n]$ is the $(Kn + k)^{th}$ element of \mathbf{v} , and \mathbf{S}_k^n is the state vector of user k at the n^{th} time instant, which can be expressed as

$$\mathbf{S}_k^n = \begin{bmatrix} x_k[n-1] & \cdots & x_k[n-J] \end{bmatrix}. \quad (40)$$

As can be noted in (40), although we need to have $L-1$ elements in the state vector for optimal sequence estimation, the number of elements in the state vector in (40), namely J , can be selected less than $L-1$, to reduce the complexity of the detector. This can be done by utilizing surviving paths constructed based on the proposed Ungerboeck type reduced state sequence estimation (U-RSSE) for MIMO with bidirectional decision feedback algorithm, the details of which will be provided in the sequel. The functions $\kappa_k^n(\cdot)$, ϕ_k^n and $\psi_{k,k'}^n(\cdot)$ in (39) are also defined as

$$\kappa_k^n(\cdot) \triangleq 2\Re \{ (v_k^*[n]x_k[n]) - x_k^*[n][\mathbf{G}[0]]_{(k,k)}x_k[n] \}, \quad (41)$$

$$\phi_k^n(\cdot) \triangleq 2\Re \{ \zeta_{k,k}[n] \}, \psi_{k,k'}^n(\cdot) \triangleq 2\Re \{ x_k^*[n][\mathbf{G}[0]]_{(k',k)}x_k[n] + \zeta_{k,k'}[n] + \zeta_{k',k}[n] \}, \quad (42)$$

where $\zeta_{k,k'}[n] = \sum_{\ell=1}^{\min(L-1,n)} x_k^*[n][\mathbf{G}[\ell]]_{(k,k')}^H x_{k'}[n-\ell]$. Here, $\kappa_k^n(\cdot)$ can be regarded as the CMF output, $\phi_k^n(\cdot)$ calculates the self-interference due to ISI, while $\psi_{k,k'}^n(\cdot)$ corresponds to the interference caused to user k from the other users. Employing (39)-(42), a metric taking into account the *a priori* probabilities of the transmitted data symbols can be found as

$$\begin{aligned} & \ln \left(\Lambda \left(\{x_k[n], \mathbf{S}_k^n\}_{\forall k,n} \mid \{v_k^n\}_{\forall k,n} \right) \right) \\ & \propto \sum_{n=0}^{N-1} \sum_{k=1}^K P(\mathbf{S}_k^0) \left\{ \kappa_k^n(v_k^n, x_k[n]) - \phi_k^n(x_k[n], \mathbf{S}_k^n) + \ln(T_k^n(x_k[n], \mathbf{S}_k^n, \mathbf{S}_k^{n+1})) \right. \\ & \quad \left. + P(\{x_k[n]\}) - \sum_{k'=1, k' < k}^K \psi_{k,k'}^n(x_k[n], \mathbf{S}_k^n, x_{k'}[n], \mathbf{S}_{k'}^n) \right\}, \quad (43) \end{aligned}$$

where $P(\{x_k[n]\})$ and $P(\mathbf{S}_k^0)$ are the *a priori* probabilities of the data symbol $x_k[n]$ and the initial state vector \mathbf{S}_k^0 . Moreover, $\ln(\cdot)$ takes the natural logarithm, and $T_k^n(x_k[n], \mathbf{S}_k^n, \mathbf{S}_k^{n+1})$ is the trellis indicator function, which is equal to 1 if a transition from \mathbf{S}_k^n to \mathbf{S}_k^{n+1} is possible with the data symbol being $x_k[n]$. Otherwise, it is equal to zero. The proposed factor graph (FG) constructed for the calculation of (43) is presented in Fig. 1. As can be noted in Fig. 1, there are cycles which are of length 6. Although the existence of cycles in the FG in Fig. 1 result in an approximate computation of (43), as it is known that the approximation errors are negligible if the length of the cycles are greater than 4 [84]. As can also be noted in Fig. 1, the state vector \mathbf{S}_k^n and the data symbol $x_k[n]$ are merged into a single variable node in order to increase the

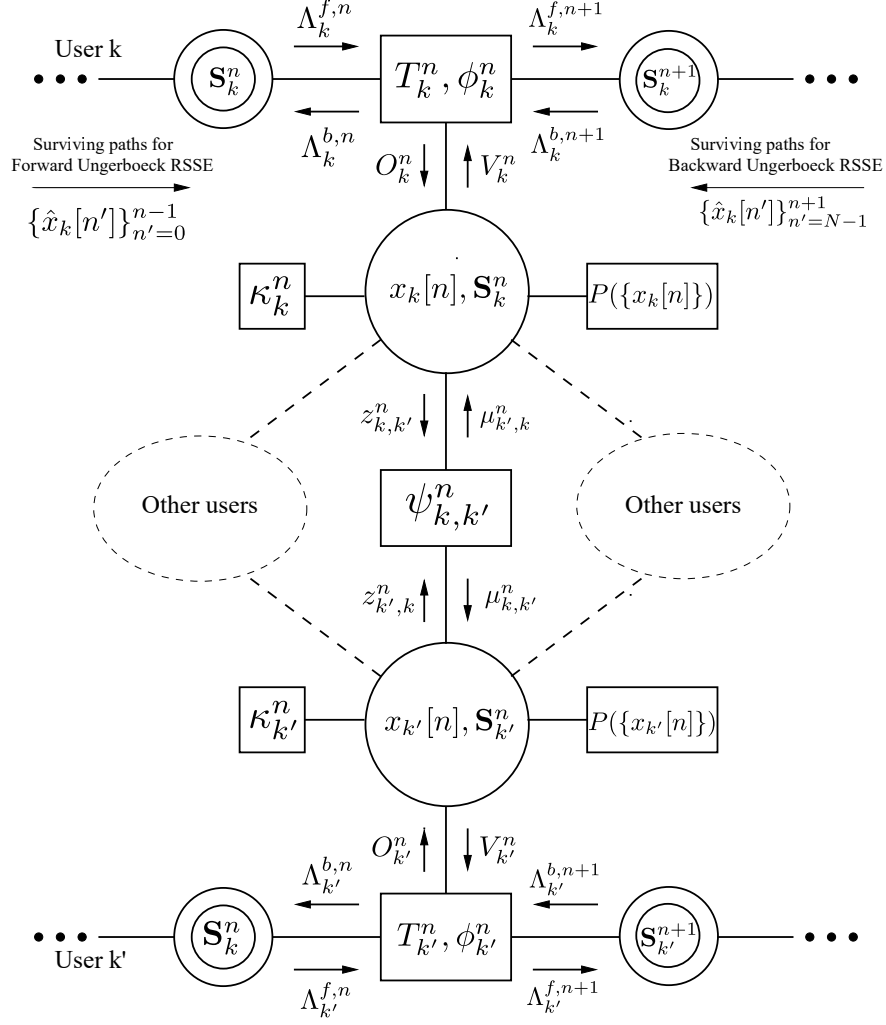


Fig. 1: Proposed factor graph corresponding to the calculation of the metric in (43).

cycle length, which is known as stretching in the literature [85]. Based on the FG in Fig. 1, a novel reduced complexity quantization-aware Ungerboeck type message passing algorithm with bidirectional decision feedback (QA-UMPA-BDF) detector is proposed, which is characterized by the following message update rules based on sum-product algorithm (SPA) framework:

$$\Lambda_k^{f,n+1}(\mathbf{S}_k^{n+1}) = \ln \left(\sum_{\sim\{\mathbf{S}_k^{n+1}\}} \exp \left(\Lambda_k^{f,n}(\mathbf{S}_k^n) + \ln(T_k^n(\cdot)) + \phi_k^n(\cdot) + V_k^n(x_k[n], \mathbf{S}_k^n) \right) \right), \quad (44)$$

$$\Lambda_k^{b,n}(\mathbf{S}_k^n) = \ln \left(\sum_{\sim\{\mathbf{S}_k^n\}} \exp \left(\Lambda_k^{b,n+1}(\mathbf{S}_k^{n+1}) + \ln(T_k^n(\cdot)) + \phi_k^n(\cdot) + V_k^n(x_k[n], \mathbf{S}_k^n) \right) \right), \quad (45)$$

$$O_k^n(x_k[n], \mathbf{S}_k^n) = \Lambda_k^{f,n}(\mathbf{S}_k^n) + \Lambda_k^{b,n+1}(\mathbf{S}_k^{n+1}) + \ln(T_k^n(\cdot)) + \phi_k^n(\cdot), \quad (46)$$

$$V_k^n(x_k[n], \mathbf{S}_k^n) = P(\{x_k[n]\}) + \kappa_k^n(\cdot) + \left[\sum_{l=1, l \neq k}^K \mu_{l,k}^n(x_k[n], \mathbf{S}_k^n) \right], \quad (47)$$

$$\mu_{k',k}^n(x_k[n], \mathbf{S}_k^n) = \ln \left(\sum_{\{x_{k'}[n]\}, \mathbf{S}_{k'}^n} \exp(z_{k',k}^n(x_{k'}[n], \mathbf{S}_{k'}^n) \psi_{k,k'}^n(\cdot)) \right), \quad (48)$$

$$z_{k',k}^n(x_k[n], \mathbf{S}_k^n) = O_k^n(x_k[n], \mathbf{S}_k^n) + V_k^n(x_k[n], \mathbf{S}_k^n) - \mu_{k',k}^n(x_k[n], \mathbf{S}_k^n), \quad (49)$$

where $\sum_{\sim\{x\}}$ is defined as the sum over all variables excluding x . Note that we calculate the messages in log domain to avoid numerical issues due to very large numbers as the multiplications performed in SPA framework are reflected as summations in log domain for the equations (44)-(49). For further avoidance of numerical issues due to large numbers, the max-log approximation [86] can be used for (44), (45) and (48) as

$$\Lambda_k^{f,n+1}(\mathbf{S}_k^{n+1}) \approx \max_{\{\mathbf{S}_k^n, x_k[n]\}} \left(\Lambda_k^{f,n}(\mathbf{S}_k^n) + \ln(T_k^n(\cdot)) + \phi_k^n(\cdot) + V_k^n(x_k[n], \mathbf{S}_k^n) \right), \quad (50)$$

$$\Lambda_k^{b,n}(\mathbf{S}_k^n) \approx \max_{\{\mathbf{S}_k^{n+1}, x_k[n]\}} \left(\Lambda_k^{b,n+1}(\mathbf{S}_k^{n+1}) + \ln(T_k^n(\cdot)) + \phi_k^n(\cdot) + V_k^n(x_k[n], \mathbf{S}_k^n) \right), \quad (51)$$

$$\mu_{k',k}^n(x_k[n], \mathbf{S}_k^n) \approx \max_{\{x_{k'}[n]\}, \mathbf{S}_{k'}^n} \left(z_{k',k}^n(x_{k'}[n], \mathbf{S}_{k'}^n) + \psi_{k,k'}^n(\cdot) \right). \quad (52)$$

Regarding the interpretation of the FG in Fig. 1, the upper part is responsible for the RSSE operation with the help of bidirectional decision feedback providing the surviving paths needed for the metric calculations. The message $\mu_{k',k}^n$ in (48) is responsible for soft multi-user interference (MUI) cancellation between user k and user k' , whereas V_k^n contains the information for the interference of all users to user k and the CMF output for the n^{th} symbol of user k .

A. Bias Compensation

Owing to the state reduction and the pre-cursor ISI remaining after CMF operation, an anti-causal interference appears. As a result, U-RSSE suffers from *correct path loss* even when there is no noise and multi-user interference [87]. This interference results in a *bias* affecting the tentative decisions in a survivor map. This bias has to be corrected in the forward surviving path construction in a similar manner as performed in [87]. With such a correction, the surviving path construction of the states of the m^{th} user can be found as

$$\hat{x}_k[n-J](\mathbf{S}_k^n) = \arg \max_{x_k[n-J]} \left[\Lambda_k^{f,n}(\mathbf{S}_k^n) + \phi_k^n(\cdot) + V_k^n(\cdot) - \beta_k^{n-J}(\mathbf{S}_k^n, x_k[n-J]) \right], \quad (53)$$

where β_k^{n-J} is the *bias* correction term. This *bias* correction term can be found by replacing $\mathbf{h}^H \mathbf{R}_g[\ell] \mathbf{h}$ matrices in our previous work [88, Eqn. (2.24)], which finds the *bias* term for a U-RSSE receiver for an unquantized single-input single-output (SISO) scenario, by $\mathbf{G}[\ell]$ in our work. In this case, the *bias* correction term can be written as

$$\beta_k^{n-J}(\mathbf{S}_k^n, x_k[n-J]) = 2 \operatorname{Re} \left\{ \sum_{k'=1}^K \left[\sum_{l_1=n-L+2}^{n-J} \sum_{l_2=n-l_1+1}^{L-1} x_k^*[l_1] [\mathbf{G}[l_2]]_{(k,k')} \tilde{x}_{k'}[l_1+l_2] \right] \right\}, \quad (54)$$

where $x_k^*[l_1]$ for $l_1 < n-j$ can be found from the surviving path constructions at the previous time instants and $\tilde{x}_{k'}[l_1+l_2]$ can also be found from the hard tentative decisions about future symbols, which are obtained in the previous iterations. The bias term is also simplified for the full decision feedback case (when no state is used, that is, when $J=0$) as

$$\beta_k^n(x_k[n]) = 2 \operatorname{Re} \left\{ \sum_{k'=1}^K \left[\sum_{l_2=1}^{L-1} \hat{x}_k^*[n] [\mathbf{G}[l_2]]_{(k,k')} \tilde{x}_{k'}[n+l_2] \right] \right\}, \quad (55)$$

since the terms of the outer summation with index $l_1 \neq n-J = n$ in (54) can be omitted as the maximization is over $x_k[n]$ in (53) for $J=0$. Ultimately, the metric in (43) can be calculated in the termination step of the SPA as

$$\ln \left(\Lambda \left(\{x_k[n], \mathbf{S}_k^n\} \mid \{v_k^n\}_{\forall k,n} \right) \right) = \sum_{\mathbf{S}_k^n} [V_k^n(\cdot) + O_k^n(\cdot) - \beta_k^n(\cdot)], \quad (56)$$

where $\beta_k^n(\cdot)$ can be calculated as

$$\beta_k^n(x_k[n], \mathbf{S}_k^n) = 2 \operatorname{Re} \left\{ \sum_{k'=1}^K \left[\sum_{l_1=n-L+J+2}^n \sum_{l_2=n-l_1+J+1}^{L-1} x_k^*[l_1] [\mathbf{G}[l_2]]_{(k,k')} \tilde{x}_{k'}[l_1+l_2] \right] \right\}. \quad (57)$$

with the corresponding data symbol estimates maximizing the metric in (43) given as

$$\hat{x}_k[n] = \arg \max_{\{x_k[n]\}} \sum_{\mathbf{S}_k^n} [V_k^n(x_k[n], \mathbf{S}_k^n) + O_k^n(x_k[n], \mathbf{S}_k^n) - \beta_k^n(x_k[n], \mathbf{S}_k^n)]. \quad (58)$$

B. Message Passing Schedule

Owing to the cycles existing in the FG in Fig. 1, there is no unique message passing schedule for SPA operation. Therefore, we employ a serial schedule as in [85] for updating the messages. The proposed scheduling for forward recursion in time-domain is presented in Algorithm 1.

When the forward recursion in time-domain presented in Algorithm 1 ends, the same procedure is performed as the backward recursion in time-domain, for which the time index at the outermost for loop in Algorithm 1 will be from $N-1$ to 0 and the operation in line 27 will be replaced by an update of backward messages in time-domain $\Lambda_k^{b,n}$ using (51), while the lines 28-29 will

Algorithm 1 QA-UMPA-BDF, forward recursion in time-domain

Input: MF output \mathbf{v} and correlation metric \mathbf{G} .

Initialization: Initialize all messages $z_{k',k}^n$, $\mu_{k',k}^n$, V_k^n , O_k^n , $\Lambda_k^{f,n}$, $\Lambda_k^{b,n}$ as zero.

```

1: for  $n = 0 : 1 : N - 1$  do
2:   for  $k = 1 : 1 : K$  do
3:     Update  $O_k^n(\cdot)$  using (46).
4:   end for
5:   Forward recursion in user domain:
6:   for  $k' = 1 : 1 : K$  do
7:     for  $k = k' + 1 : 1 : K$  do
8:       Update  $\{\mu_{k',k}^n\}$  using (52).
9:     end for
10:    Update the term  $V_k^n(\cdot)$  using (47).
11:    for  $k = 1 : 1 : k' - 1$  do
12:      Update  $\{z_{k,k'}^n\}$  using (49).
13:    end for
14:  end for
15:  Backward recursion in user domain:
16:  for  $k = K : -1 : 1$  do
17:    for  $k' = K : -1 : k + 1$  do
18:      Update  $\{\mu_{k',k}^n\}$  using (52).
19:    end for
20:    Update the term  $V_k^n(\cdot)$  using (47).
21:    for  $k' = k - 1 : -1 : 1$  do
22:      Update  $\{z_{k,k'}^n\}$  using (49).
23:    end for
24:  end for
25:  Update the time-domain forward messages:
26:  for  $k = 1 : 1 : K$  do
27:    Update  $\Lambda_k^{f,n+1}(\cdot)$  using (50).
28:    Calculate bias term  $\beta_k^{n-J}(\mathbf{S}_k^n, x_k[n-J])$  using (54) or (55).
29:    Update surviving paths  $\hat{x}_k[n-J](\mathbf{S}_k^n)$  using (53).
30:  end for
31: end for

```

not be performed. Completion of forward and backward recursions in time-domain ends a single iteration of the QA-UMPA-BDF detector. Although various choices can be made for the stopping criteria, the one adopted in this study is the completion of a predefined number of iterations (I). The initialization step in Algorithm 1 should only be performed for the forward recursion in time-domain in the first iteration.

C. Computational Complexity Analysis

The computational complexity per iteration of the proposed QA-UMPA-BDF detector can be found by analyzing (44)-(54). For the complexity analysis we consider the max-log approximations for (44), (45) and (48), which are (50), (51), (52). The complexity to calculate the messages per single iteration of the proposed detector is provided in Table I. As can be noted from Table I,

	(46)	(47)	(49)	(50), (51), (53)	(52)	(54)
Complexity	$\mathcal{O}(NPKL)$	$\mathcal{O}(NPK^2)$	$\mathcal{O}(NPK)$	$\mathcal{O}(NP^{(J+1)}K)$	$\mathcal{O}(NP^{2(J+1)}K)$	$\mathcal{O}(NP^{(J+1)}K^2L)$

TABLE I: Computational complexity of the QA-UMPA-BDF detector per iteration.

the computational complexity per iteration can be as high as $\mathcal{O}(NP^{2(L+1)}K)$ if reduced state estimation is not employed (when $J = L - 1$). However, the computational complexity can be reduced to $\mathcal{O}(NPKL) + \mathcal{O}(NPK^2) + \mathcal{O}(NPK) + \mathcal{O}(NPK) + \mathcal{O}(P^2K) + \mathcal{O}(NPK^2L)$, which changes linearly with almost all parameters, except K and P , for which there is a quadratic increase in complexity. The complexity to calculate CMF output \mathbf{v} and the correlation metric \mathbf{G} are $\mathcal{O}(MKNL)$ and $\mathcal{O}(MK^2L)$, which are excluded from discussion as they are only calculated once, not per iteration. In the representative benchmark algorithm that we compare the proposed QA-UMPA-BDF detector, namely the ‘‘Robust MMSE’’ in [66, Eqn.(27)], the computational complexity is $\mathcal{O}(MKN \log_2(N)) + \mathcal{O}(MK) + \mathcal{O}(MK^2) + \mathcal{O}(NK^3)$, whose complexity is growing with K^3 . Therefore, it can be stated that the proposed QA-UMPA-BDF detector for $J = 0$ has lower complexity compared to the benchmark detector, especially when K is large. We will also show in Section VII that the proposed detector can converge in about $I = 2$ iterations for most of the cases. Therefore, the number of iterations does not increase the proposed detector complexity to a significant degree. Lower complexity detectors compared to the ‘‘Robust MMSE’’ detector are also proposed in [66]. However, their performance is inferior compared to ‘‘Robust MMSE’’ detector [66, Fig.12], thus ‘‘Robust MMSE’’ is chosen as the benchmark detector.

VI. PERFORMANCE METRICS

To assess the performance of the proposed LMMSE channel estimator, normalized MSE curves are plotted. The normalized MSE taking into account the channel coefficients multiplied by the power delay profile can be found as [89]

$$\text{nMSE} = \frac{\text{Tr} \left[\mathbf{\Omega} \mathbf{C}_{\hat{\mathbf{h}}}^{\text{LME}} \mathbf{\Omega}^H \right]}{\text{Tr} \left[\mathbf{\Omega} \mathbf{C}_{\mathbf{h}} \mathbf{\Omega}^H \right]} = \frac{\text{Tr} \left[\mathbf{\Omega} \mathbf{C}_{\hat{\mathbf{h}}}^{\text{LME}} \mathbf{\Omega}^H \right]}{MK}, \quad (59)$$

where $\mathbf{\Omega}$ is a diagonal matrix whose $(ML(k-1) + M\ell + 1)^{\text{th}}$ to $(ML(k-1) + M\ell + M)^{\text{th}}$ diagonal elements are all equal to $\sqrt{\rho_k[\ell]}$. $\mathbf{C}_{\hat{\mathbf{h}}}^{\text{LME}}$ can be found by (21), (26) or (27). For the data detector performance metric, we use bit-error-rate (BER) and average mismatched achievable rate (AIR) per user [90], which is a suitable metric to assess the performance of mismatched decoders, employing approximate *a posteriori* probabilities (APP), as the exact APPs cannot be calculated due to the cycles in the FG in Fig. 1 and Gaussian effective noise approximations. The mismatched AIR can be expressed as [90]

$$\text{AIR} = \mathbb{E}_{\mathbf{x}, \mathbf{H}} \left[\frac{1}{NK} \sum_{k=1}^K \sum_{n=0}^{N-1} \left[\log_2(P) - \log_2 \left(\frac{\sum_{x'_k[n] \in A_x} \tilde{p}(\mathbf{v} | x'_k[n])}{\tilde{p}(\mathbf{v} | \hat{x}_k[n] = x_k[n])} \right) \right] \right], \quad (60)$$

where A_x is the set of all possible constellation points and $\tilde{p}(\mathbf{v} | x_k[n])$ are the approximate APPs which are found using (58) as

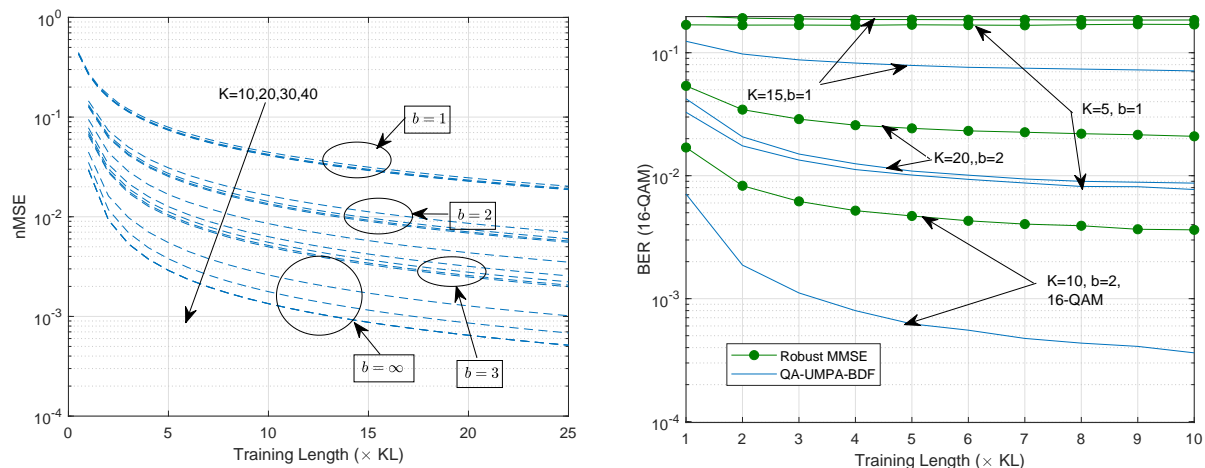
$$\tilde{p}(\mathbf{v} | x_k[n]) = \sum_{\mathbf{S}_k^n} \exp(V_k^n(x_k[n], \mathbf{S}_k^n) + O_k^n(x_k[n], \mathbf{S}_k^n) - \beta_k^n(x_k[n], \mathbf{S}_k^n)). \quad (61)$$

VII. SIMULATION RESULTS

In this section, we will present the normalized MSE (nMSE), BER and AIR performance of the proposed QA-UMPA-BDF detector. We will concentrate on the performance comparison between the proposed QA-UMPA-BDF detector and the representative robust MMSE detector [66] from the literature, which has comparable complexity to our detector, as the reduced state length of the QA-UMPA-BDF detector is set as $J = 0$. We will see that the proposed detector outperforms the representative detector in all cases, even if their complexities are similar and the QA-UMPA-BDF detector provides a higher spectral efficiency, due to the absence of a cyclic-prefix. Unless otherwise stated, $M = 100$, the power-delay profile of the transmission channel is COST-207 typical delay profile for suburban and urban areas [91]. The number of channel taps $L = 32$, with the power ratio of the first and the last taps being 30 dB. The number of iterations for the QA-UMPA-BDF detector is selected as 2. The pilot symbols are created as

random complex numbers from QPSK modulation. $E_b \triangleq E_s/\log_2(P)$ corresponds to the bit-energy. LMMSE channel estimates and MSE values are found based on (25) and (26). The step size of the quantizer is selected to optimally to minimize quantization noise as in [37].

To determine the necessary training length for the channel estimation, the nMSE or BER vs. the training length (τ) performances are obtained as in Fig. 2. In Fig. 2a, we observe that if we



(a) nMSE vs. training length (τ), $K = 10, 20, 30, 40$, $E_b/N_o = 0$ dB.

(b) BER vs. training length, $K = 5, 10, 15, 20$, $E_b/N_o = 0$ dB, (16-QAM)

Fig. 2: nMSE (a) and BER (b) vs. training length (τ)

need to have a nMSE level less than 10^{-1} , $\tau \geq 5KL$ will be an adequate choice for the proposed LMMSE channel estimator for one-bit quantizer, although this number is much less for higher bit resolutions. However, we can also say that there is a decreased improvement for nMSE if the training length $\tau > 5KL$ for any bit resolution. Nevertheless, observing nMSE alone may not be enough to foresee how the error-rate performance of the proposed detector changes with the training length. Therefore, BER vs. training length is also obtained for 16-QAM modulated data symbols as in Fig. 2b. As can be noted in Fig. 2b, for 1 and 2 bits, there is a significant error-floor advantage of the proposed detector compared to the Robust MMSE detector [66] for all cases. Moreover, we can see that with very low resolution quantizers (1 or 2 bits), increasing τ more than $5KL$ is not very effective for decreasing BER. Therefore, we will set $\tau = 5KL$ when $q = 1, 2$. For $q = 3$, we will set $\tau = 3KL$ observing nMSE values close to 10^{-2} from Fig. 2, which is considered to be adequate. For larger bit resolutions, τ will be selected as $2KL$ in the subsequent simulations, all performed under imperfect channel state information (CSI).

In in Fig. 3, we compare the BER performance of the proposed QA-UMPA-BDF and the Robust MMSE [66] detectors in Fig. 3 for either QPSK with $q = 1$ or 16-QAM with $q = 2$. We also include the performance of a genie aided detector, which calculates the metric in (43) for an $x_k[n]$ assuming that all other symbols are perfectly known so that the terms corresponding to the ISI and MUI cancellation in (43) are calculated accordingly. Genie aided detector performance is mainly limited by thermal and quantization noise and named ‘‘Genie Aided Det.’’ in all figures.

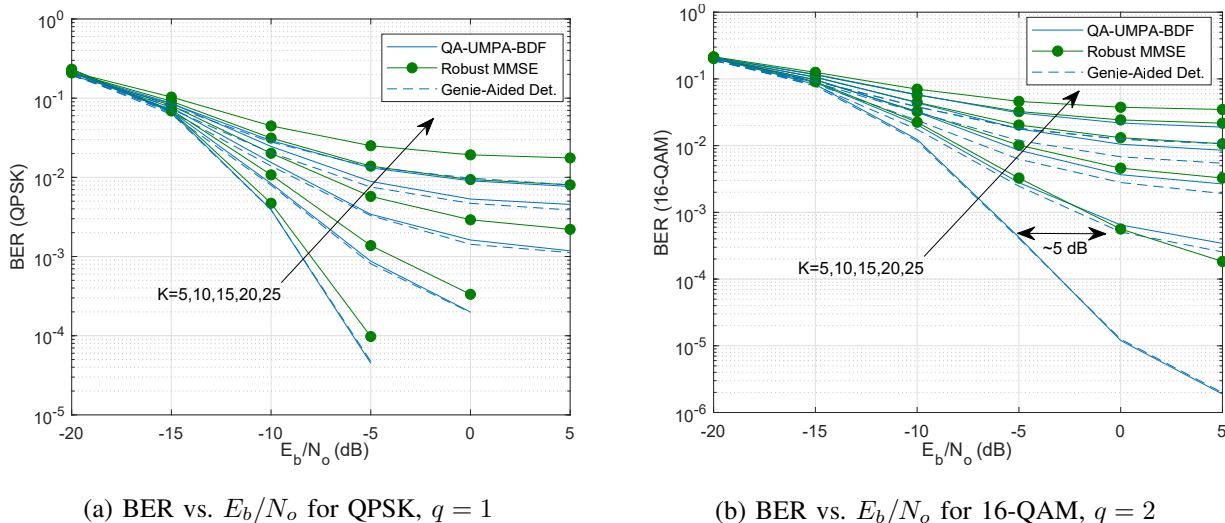


Fig. 3: BER vs. E_b/N_o for QPSK, $q = 1$ (a) or 16-QAM, $q = 2$ (b).

As can be noted in Fig. 3a, the QA-UMPA-BDF detector has better performance compared to the representative benchmark detector for all number of user values (for $K = 5, 10, \dots, 25$), despite being spectrally more efficient due the CP free transmission. If the modulation type is changed to 16-QAM, the SNR advantage of QA-UMPA-BDF is up to 5 dB as can be noted in Fig. 3b. Moreover, the QA-UMPA-BDF detector performance is very close to the genie-aided detector in all cases, supporting that two iterations with QA-UMPA-BDF detector is enough to achieve the genie-aided detector, which will also hold for the most of subsequent simulations.

As the next simulation scenario, we plot the error-rate performances for fixed K but varying q in Fig. 4. For all cases, again QA-UMPA-BDF has better performance, where the performance gap between the two detectors is widened for 16-QAM. For QPSK, performance improvement is not much for $q > 2$, whereas $q = 3$ seems to be an enough for 16-QAM. Again, two iterations for QA-UMPA-BDF is observed to be sufficient to attain genie-aided detector performance.

In the next simulation setting, the BER performances are observed for various modulation

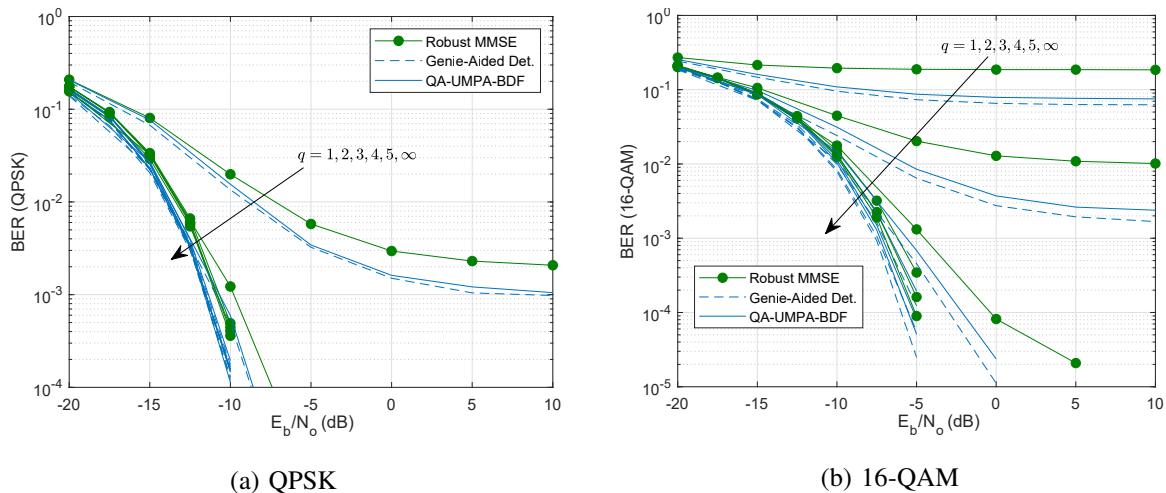


Fig. 4: BER vs. SNR $K = 15$, $q = 1, 2, 3, 4, 5, \infty$ for QPSK (a), 16-QAM (b).

orders (16-QAM, 8-PSK, 4-PSK and BPSK) in Fig.5. Again, QA-UMPA-BDF has better performance compared to the benchmark detector for all modulation types, with significant performance difference for 16-QAM modulation. The reason to observe different BER for BPSK and QPSK is due to the correlation in the noise statistics stemming from the nonlinear quantizer. Such BER performance difference between BPSK and QPSK under quantization is also reported in [92].

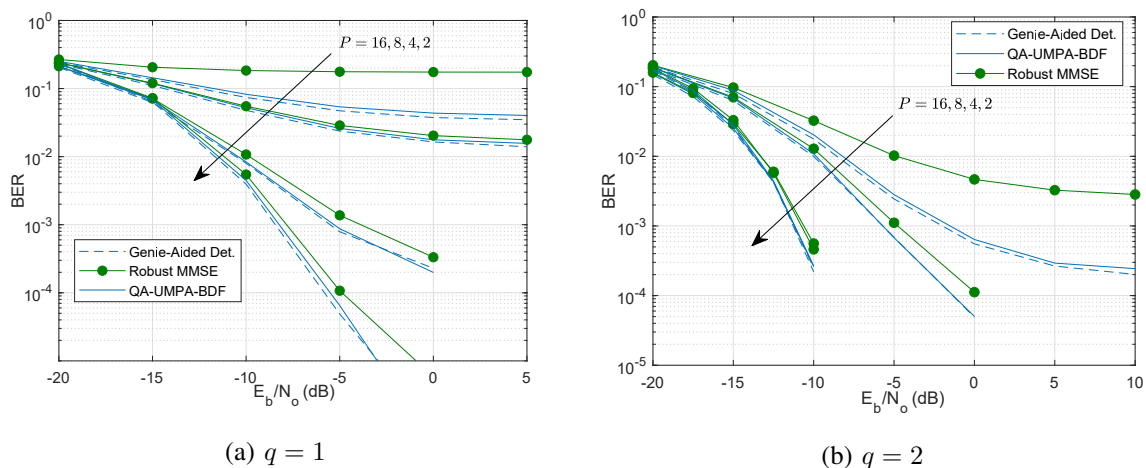


Fig. 5: BER vs. SNR for $P = 16, 8, 4, 2$, $K = 10$, $q = 1$ (a) and $q = 2$ (b)

We also obtain per user AIR vs. SNR curves for $b = 1$ and $b = 2$ in Fig. 6. In Fig. 6, QA-UMPA-BDF detector provides an AIR about 2.8 bit per channel use (bpcu) with $q = 1$,

which is close to the maximum AIR per user of 3 bpcu for 8-PSK. With 64-QAM, the AIR can be up to 3.5 bpcu for $q = 1$. When $q = 2$, we can see from Fig. 6b that up to 5.5 bpcu can be achieved with 64-QAM, which is close to the maximum AIR value of 6 bpcu for 64-QAM.

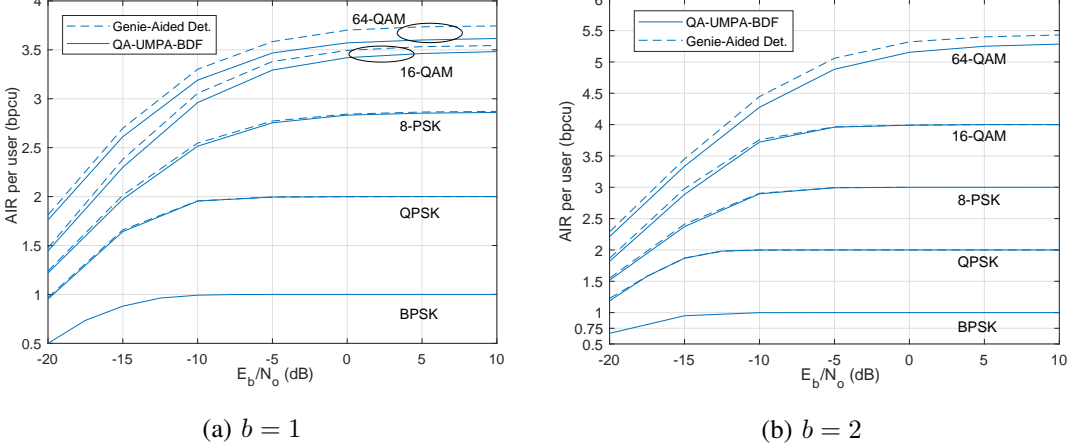


Fig. 6: Per user AIR vs. E_b/N_o , $K = 10$, $b = 1$ (a), $b = 2$ (b).

In the next simulation setting, we obtain the total AIR instead of per user AIR vs. the number of users (K) in Fig. 7 when $E_b/N_o = 0$ dB, $M = 50$, $I = 7$ and the power delay profile is uniform. The key takeaways from Fig. 7 are as follows:

- Strong total AIR performance is observed with QPSK even with $q = 2$ and a very loaded case of 60 users, which is more than the number of antennas (maximum possible total AIR for 60 users is 120 bpcu with QPSK). Total AIR always rise with increasing K .
- For 8-PSK, total AIR is better than QPSK for all q , if not similar. For $q = 4$ maximum total AIR performance is achieved even with $K = 60$. Total AIR always rise with increasing K .
- For $q < 4$ with 16-QAM, total AIR always increase with K . For $q \geq 4$, the maximum total AIR is observed for $K \approx 45, 53, 57$. Competitive performance with no degradation for up to about 55 users is observed for $q > 4$. Depending on the number of bits and users, 16-QAM has better total AIR performance than QPSK or 8-PSK in many cases.
- 64-QAM has better total AIR performance compared to other modulation types for $q > 4$ and $K < 35$. For higher K and lower q , smaller modulation orders provide better total AIR performance in some cases. The maximum total AIR is similar to that of 16-QAM.

For the final simulation cases, we present the BER performance when the number of channel taps are varied in Fig. 8a and the AIR per user performance vs. number of ADC bits for

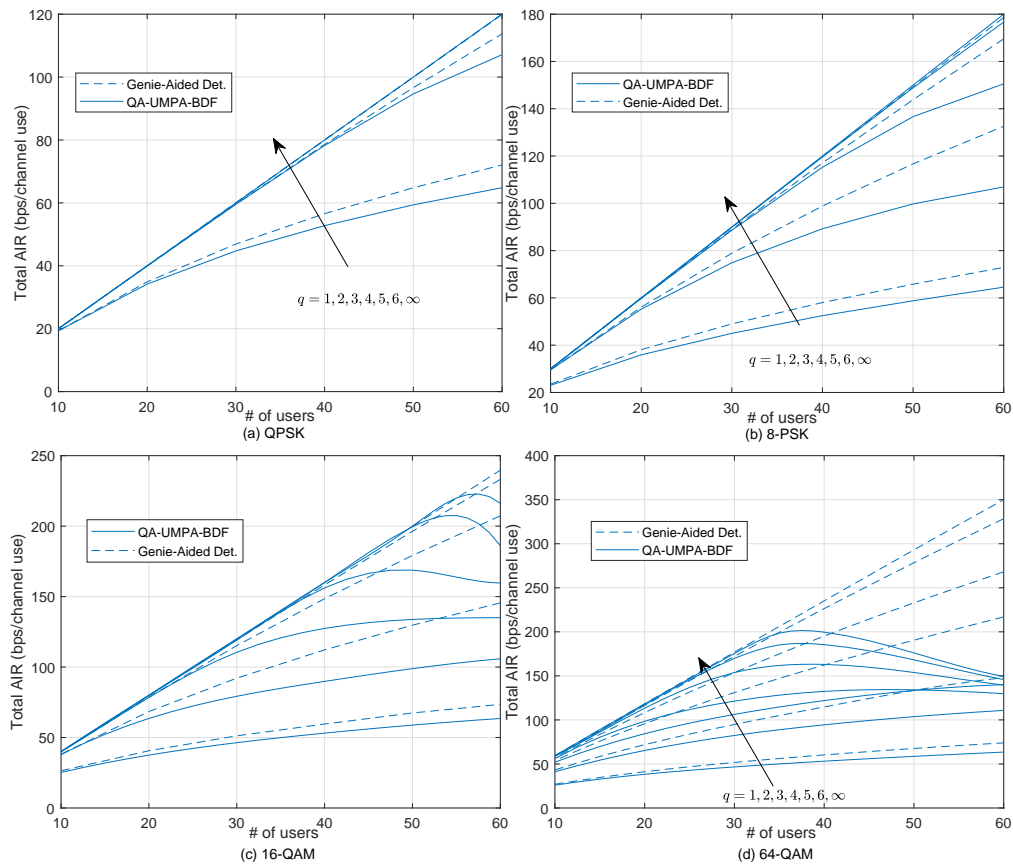


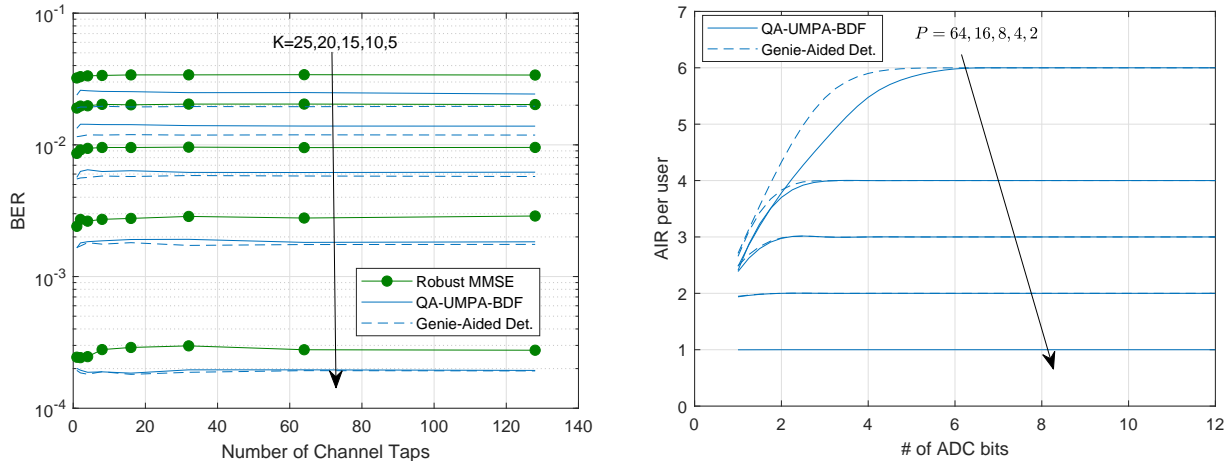
Fig. 7: Total AIR vs. Number of users, $M = 50$, $E_b/N_o = 0$ dB, $q = 1, 2, \dots, 6, \infty$, QPSK (a), 8-PSK (b), 16-QAM (c), 64-QAM (d).

$E_b/N_o = 0$ dB and $I = 7$ in Fig. 8b. In Fig. 8a, it can be seen that the proposed QA-UMPA-BDF detector has a very robust BER performance to the changes in the number of channel taps. It can cancel ISI in time-domain effectively even when the number of channel taps is as large as 128. It also has better performance compared to the representative detector for all cases.

In Fig. 8b, it can be stated that 64-QAM modulation can be used with the maximum possible AIR per user if $q > 5$, while the maximum possible AIR is achieved for $q > 2$ with 16-QAM. QA-UMPA-BDF detector can provide higher AIR per user values for 64-QAM if $q > 2$ for $K = 25$. If $q \leq 2$, either 64-QAM or 16-QAM can be used as their AIR per user is similar.

VIII. CONCLUSIONS

In this paper, we proposed an LMMSE channel estimation and a quantization-aware message passing low-complexity detector based on bidirectional decision feedback. The proposed detector



(a) BER vs. L for $E_b/N_o = 0$ dB, $b = 1$, QPSK modulation.

(b) Per user AIR vs. number of bits q for $K = 25$, $E_b/N_o = 0$ dB.

Fig. 8: BER vs. number of channel taps L (a) or per user AIR vs. number of bits q (b).

has very low complexity compared to the existing work in the literature for highly dispersive channels with large number of channel taps, thanks to its reduced state sequence estimation capability. Under imperfect CSI conditions, the proposed QA-UMPA-BDF detector is compared with a representative detector from the literature with a comparable complexity but having lower spectral efficiency due to its requirement to use a cyclic-prefix. The proposed QA-UMPA-BDF detector is observed to outperform the representative detector in all examined cases, for some of which the performance differences are significant.

REFERENCES

- [1] E. G. Larsson *et al.*, “Massive MIMO for next generation wireless systems,” *IEEE Commun. Mag.*, vol. 52, no. 2, pp. 186–195, Feb. 2014.
- [2] L. Lu, G. Y. Li, A. L. Swindlehurst, A. Ashikhmin, and R. Zhang, “An overview of massive mimo: Benefits and challenges,” *IEEE J. Sel. Topics Signal Process.*, vol. 8, no. 5, pp. 742–758, 2014.
- [3] A. B. Üçüncü and A. O. Yılmaz, “Performance analysis of faster than symbol rate sampling in 1-bit massive MIMO systems,” in *Proc. IEEE Int. Conf. Commun.*, 2017, pp. 1–6.
- [4] T. L. Marzetta, E. G. Larsson, Y. Hong, and H. Q. Ngo, *Fundamentals of massive MIMO*, 2016.
- [5] A. B. Üçüncü, E. Björnson, H. Johansson, A. O. Yılmaz, and E. G. Larsson, “Performance analysis of quantized uplink massive MIMO-OFDM with oversampling under adjacent channel interference,” *IEEE Trans. Commun.*, vol. 68, no. 2, pp. 871–886, 2020.
- [6] A. B. Üçüncü and A. O. Yılmaz, “Uplink performance analysis of oversampled wideband massive MIMO with one-bit ADCs,” in *Proc. 2018 IEEE 88th Veh. Technol. Conf.*

- [7] S. Jacobsson *et al.*, “Throughput analysis of massive MIMO uplink with low-resolution ADCs,” *IEEE Trans. Wireless Commun.*, vol. 16, no. 6, pp. 4038–4051, Jun. 2017.
- [8] S. Jacobsson *et al.*, “One-bit massive MIMO: Channel estimation and high-order modulations,” in *Proc. IEEE Int. Conf. Commun.*, London, 2015, pp. 1304–1309.
- [9] A. B. Üçüncü and A. O. Yılmaz, “Oversampling in one-bit quantized massive MIMO systems and performance analysis,” *IEEE Trans. Wireless Commun.*, vol. 17, no. 12, pp. 7952–7964, Dec. 2018.
- [10] A. B. Üçüncü, E. Björnson, H. Johansson, A. O. Yılmaz, and E. G. Larsson, “Performance of one-bit massive MIMO with oversampling under adjacent channel interference,” in *Proc. IEEE Global Commun. Conf.*, 2019, pp. 1–6.
- [11] A. B. Üçüncü and A. O. Yılmaz, “Sequential linear detection in one-bit quantized uplink massive MIMO with oversampling,” in *Proc. IEEE 88th Veh. Technol. Conf.*, 2018.
- [12] A. Mezghani, F. Antreich, and J. A. Nossek, “Multiple parameter estimation with quantized channel output,” in *Proc. Int. ITG Workshop Smart Antennas*, 2010, pp. 143–150.
- [13] A. Mezghani and J. A. Nossek, “Efficient reconstruction of sparse vectors from quantized observations,” in *Proc. Int. ITG Workshop Smart Antennas*, 2012, pp. 193–200.
- [14] J. Mo, P. Schniter, N. G. Prelcic, and R. W. Heath, “Channel estimation in millimeter wave MIMO systems with one-bit quantization,” in *Proc. Asilomar Conf. Signals, Syst. Comput.*, 2014, pp. 957–961.
- [15] J. Choi, D. J. Love, and D. R. Brown, “Channel estimation techniques for quantized distributed reception in MIMO systems,” in *Proc. Asilomar Conf. Signals, Syst. Comput.*, 2014, pp. 1066–1070.
- [16] J. Choi, J. Mo, and R. W. Heath, “Near maximum-likelihood detector and channel estimator for uplink multiuser massive MIMO systems with one-bit ADCs,” *IEEE Trans. Commun.*, vol. 64, no. 5, pp. 2005–2018, May. 2016.
- [17] C. Risi *et al.* (2014, Apr. 30) *Massive MIMO with 1-bit ADC*. [Online]. Available: <http://arxiv.org/abs/1404.7736>
- [18] C. Wen, C. Wang, S. Jin, K. Wong, and P. Ting, “Bayes-optimal joint channel-and-data estimation for massive MIMO with low-precision ADCs,” *IEEE Trans. Signal Process.*, vol. 64, no. 10, pp. 2541–2556, May 2016.
- [19] Z. Zhou, X. Chen, D. Guo, and M. L. Honig, “Sparse channel estimation for massive MIMO with 1-bit feedback per dimension,” in *Proc. Wireless Commun. Netw. Conf.*, 2017, pp. 1–6.
- [20] H. Kim and J. Choi, “Channel estimation for one-bit massive MIMO systems exploiting spatio-temporal correlations,” in *Proc. Global Commun. Conf.*, 2018, pp. 1–6.
- [21] C. Rusu, R. Mendez-Rial, N. Gonzalez-Prelcic, and R. W. Heath, “Adaptive one-bit compressive sensing with application to low-precision receivers at mmwave,” in *Proc. Global Commun. Conf.*, 2015, pp. 1–6.
- [22] J. Rodriguez-Fernandez, N. Gonzalez-Prelcic, and R. W. Heath, “Channel estimation in mixed hybrid-low resolution MIMO architectures for mmwave communication,” in *2016 50th Asilomar Conf. Signals, Syst. Comput.*, 2016, pp. 768–773.
- [23] J. Sung, J. Choi, and B. L. Evans, “Narrowband channel estimation for hybrid beamforming millimeter wave communication systems with one-bit quantization,” in *Proc. Int. Conf. Acoust., Speech Signal Process.*, 2018, pp. 3914–3918.
- [24] S. Rao, G. Seco-Granados, H. Pirzadeh, and A. L. Swindlehurst. (2020, May 15) *Massive MIMO Channel Estimation with Low-Resolution Spatial Sigma-Delta ADCs*. [Online]. Available: <https://arxiv.org/abs/2005.07752>
- [25] Q. Wan, J. Fang, H. Duan, Z. Chen, and H. Li, “Generalized bussgang LMMSE channel estimation for one-bit massive MIMO systems,” *IEEE Trans. Wireless Commun.*, vol. 19, no. 6, pp. 4234–4246, Jun. 2020.
- [26] M. Y. Takeda, A. Klautau, A. Mezghani, and R. W. Heath, “MIMO channel estimation with non-ideal ADCs: Deep learning versus GAMP,” in *Proc. IEEE Int. Workshop Machine Learning for Signal Process.*, 2019, pp. 1–6.
- [27] Y.-S. Jeon, J. Li, N. Tavangaran, and H. V. Poor. (2020, Mar. 23) *Data-aided channel estimator for MIMO systems via reinforcement learning*. [Online]. Available: <https://arxiv.org/abs/2005.07752>

- [28] N. J. Myers and R. W. Heath, "A compressive channel estimation technique robust to synchronization impairments," in *Proc. Int. Workshop Signal Process. Adv. Wireless Commun.*, 2017, pp. 1–5.
- [29] N. J. Myers and R. W. Heath, "Joint CFO and channel estimation in millimeter wave systems with one-bit ADCs," in *Proc. Int. Workshop Comput. Adv. Multi-Sensor Adapt. Process.*, 2017, pp. 1–5.
- [30] L. Xu, F. Gao, and C. Qian. (2019, Sep. 23) Gridless angular domain channel estimation for mmwave massive MIMO system with one-bit quantization via approximate message passing. [Online]. Available: <https://arxiv.org/abs/1909.10114>
- [31] J. Choi, Y. Cho, B. L. Evans, and A. Gatherer, "Robust learning-based ml detection for massive MIMO systems with one-bit quantized signals," in *Proc. Global Commun. Conf.*, Dec. 2019, pp. 1–6.
- [32] M. Masood, L. H. Afify, and T. Y. Al-Naffouri, "Efficient coordinated recovery of sparse channels in massive MIMO," *IEEE Trans. Signal Process.*, vol. 63, no. 1, pp. 104–118, Jun. 2015.
- [33] C. Steckle, J. Munir, A. Mezghani, and J. A. Nossek, "Channel estimation in massive MIMO systems using 1-bit quantization," in *Proc. Int. Workshop Signal Process. Adv. Wireless Commun.*, 2016, pp. 1–6.
- [34] C. Mollen *et al.*, "Uplink performance of wideband massive MIMO with one-bit ADCs," *IEEE Trans. Wireless Commun.*, vol. 16, no. 1, pp. 87–100, Jan. 2017.
- [35] Y. Li *et al.*, "Channel estimation and performance analysis of one-bit massive MIMO systems," *IEEE Trans. Signal Process.*, vol. 65, no. 15, pp. 4075–4089, Aug. 2017.
- [36] Chen Cao, Hongxiang Li, and Zixia Hu, "An amp based decoder for massive MU-MIMO-OFDM with low-resolution ADCs," in *Proc. Int. Conf. Comput., Netw. Commun.*, 2017, pp. 449–453.
- [37] J. Mo, P. Schniter, and R. W. Heath, "Channel estimation in broadband millimeter wave MIMO systems with few-bit ADCs," *IEEE Trans. Signal Process.*, vol. 66, no. 5, pp. 1141–1154, Mar. 2018.
- [38] A. Mezghani and A. L. Swindlehurst, "Blind estimation of sparse broadband massive MIMO channels with ideal and one-bit ADCs," *IEEE Trans. Signal Process.*, vol. 66, no. 11, pp. 2972–2983, Jun. 2018.
- [39] Y. Wang, W. Xu, H. Zhang, and X. You, "Wideband mmwave channel estimation for hybrid massive MIMO with low-precision ADCs," *IEEE Wireless Commun. Lett.*, vol. 8, no. 1, pp. 285–288, Feb. 2019.
- [40] N. J. Myers and R. W. Heath, "Message passing-based joint CFO and channel estimation in mmwave systems with one-bit ADCs," *IEEE Trans. Wireless Commun.*, vol. 18, no. 6, pp. 3064–3077, 2019.
- [41] A. L. S. Ly. V. Nguyen. (2020, Mar. 24) SVM-based Channel Estimation and Data Detection for One-Bit Massive MIMO Systems. [Online]. Available: <https://arxiv.org/abs/2003.10678>
- [42] S. Wang, Y. Li, and J. Wang, "Multiuser detection in massive MIMO with quantized phase-only measurements," in *Proc. Int. Conf. Commun.*, 2015, pp. 4576–4581.
- [43] H. G. Myung, J. Lim, and D. J. Goodman, "Peak-to-average power ratio of single carrier FDMA signals with pulse shaping," in *Proc. Int. Symp. Personal, Indoor Mobile Radio Commun.*, 2006, pp. 1–5.
- [44] F. Pancaldi, G. M. Vitetta, R. Kalbasi, N. Al-Dhahir, M. Uysal, and H. Mheidat, "Single-carrier frequency domain equalization," *IEEE Signal Process. Mag.*, vol. 25, no. 5, pp. 37–56, Sep. 2008.
- [45] O. T. Demir and E. Björnson, "Admm-based one-bit quantized signal detection for massive MIMO systems with hardware impairments," in *Proc. IEEE Int. Conf. Acoust., Speech Signal Process.*, 2020, pp. 9120–9124.
- [46] Y. Xiong, N. Wei, and Z. Zhang, "A low-complexity iterative gamp-based detection for massive MIMO with low-resolution ADCs," in *Proc. IEEE Wireless Commun. Netw. Conf.*, 2017, pp. 1–6.
- [47] Y. Jeon, M. So, and N. Lee, "Reinforcement-learning-aided ML detector for uplink massive MIMO systems with low-precision ADCs," in *Proc. IEEE Wireless Commun. and Netw. Conf.*, 2018, pp. 1–6.
- [48] J. Choi, Y. Cho, B. L. Evans, and A. Gatherer, "Robust learning-based ML detection for massive MIMO systems with one-bit quantized signals," in *Proc. IEEE Global Commun. Conf.*, 2019, pp. 1–6.

- [49] F. Steiner, A. Mezghani, L. Swindlehurst, J. A. Nossek, and W. Utschick, "Turbo-like joint data-and-channel estimation in quantized massive MIMO systems," in *Proc. Int. ITG Workshop Smart Antennas*, 2016, pp. 1–5.
- [50] Z. Zhang, X. Cai, C. Li, C. Zhong, and H. Dai, "One-bit quantized massive MIMO detection based on variational approximate message passing," *IEEE Trans. Signal Process.*, vol. 66, no. 9, pp. 2358–2373, 2018.
- [51] L. V. Nguyen *et al.*, "Supervised and semi-supervised learning for MIMO blind detection with low-resolution ADCs," *IEEE Trans. Wireless Commun.*, vol. 19, no. 4, pp. 2427–2442, Apr. 2020.
- [52] K. In-soo and J. Choi, "Channel estimation via gradient pursuit for mmwave massive MIMO systems with one-bit ADCs," *EURASIP J. Wireless Commun. Netw.*, vol. 2019, no. 1, p. 289, Dec. 2019.
- [53] Y. Jeon, N. Lee, and H. V. Poor, "Reinforcement-learning-aided detector for time-varying MIMO systems with one-bit ADCs," in *Proc. IEEE Global Commun. Conf.*, 2019, pp. 1–6.
- [54] D. Kim, S. Hong, and N. Lee, "Supervised-learning for multi-hop MU-MIMO communications with one-bit transceivers," *IEEE J. Sel. Areas Commun.*, vol. 37, no. 11, pp. 2559–2572, Nov. 2019.
- [55] C. Wen, C. Wang, S. Jin, K. Wong, and P. Ting, "Bayes-optimal joint channel-and-data estimation for massive MIMO with low-precision ADCs," *IEEE Trans. Signal Process.*, vol. 64, no. 10, pp. 2541–2556, May. 2016.
- [56] S. Wang, L. Zhang, Y. Li, J. Wang, and E. Oki, "Multiuser MIMO transmission aided by massive one-bit magnitude measurements," *IEEE Trans. Wireless Commun.*, vol. 15, no. 10, pp. 7058–7073, Oct. 2016.
- [57] Z. Zhang, X. Cai, C. Li, C. Zhong, and H. Dai, "One-bit quantized massive MIMO detection based on variational approximate message passing," *IEEE Trans. Signal Process.*, vol. 66, no. 9, pp. 2358–2373, May. 2018.
- [58] Y. Jeon, S. Hong, and N. Lee, "Supervised-learning-aided communication framework for MIMO systems with low-resolution ADCs," *IEEE Trans. Veh. Technol.*, vol. 67, no. 8, pp. 7299–7313, Aug. 2018.
- [59] J. Choi, D. J. Love, D. R. Brown, and M. Boutin, "Quantized distributed reception for MIMO wireless systems using spatial multiplexing," *IEEE Trans. Signal Process.*, vol. 63, no. 13, pp. 3537–3548, Jul. 2015.
- [60] C. Studer and G. Durisi, "Quantized massive MU-MIMO-OFDM uplink," *IEEE Trans. Commun.*, vol. 64, no. 6, pp. 2387–2399, Jun. 2016.
- [61] H. He, C. Wen, and S. Jin, "Bayesian optimal data detector for hybrid mmwave MIMO-OFDM systems with low-resolution ADCs," *IEEE J. Sel. Topics Signal Process.*, vol. 12, no. 3, pp. 469–483, Jun. 2018.
- [62] S. Wang, Y. Li, and J. Wang, "Multiuser detection for uplink large-scale MIMO under one-bit quantization," in *Proc. IEEE Int. Conf. Commun.*, 2014, pp. 4460–4465.
- [63] S. Wang, L. Zhang, Y. Li, J. Wang, and E. Oki, "Multiuser MIMO communication under quantized phase-only measurements," *IEEE Trans. Commun.*, vol. 64, no. 3, pp. 1083–1099, Mar. 2016.
- [64] J. Garcia, J. Munir, R. Kilian, and J. A. Nossek. (2016, Sep. 15) *Channel estimation and data equalization in frequency-selective MIMO systems with one-bit quantization*. [Online]. Available: <https://arxiv.org/abs/1609.04536>
- [65] S. Wang, Y. Li, and J. Wang, "Multiuser detection in massive spatial modulation MIMO with low-resolution ADCs," *IEEE Trans. Wireless Commun.*, vol. 14, no. 4, pp. 2156–2168, Apr. 2015.
- [66] J. Guerreiro, R. Dinis, and P. Montezuma, "Low-complexity sc-fde techniques for massive MIMO schemes with low-resolution ADCs," *IEEE Trans. Commun.*, vol. 67, no. 3, pp. 2368–2380, Mar. 2019.
- [67] Y. Jeon, N. Lee, S. Hong, and R. W. Heath, "One-bit sphere decoding for uplink massive MIMO systems with one-bit ADCs," *IEEE Trans. Wireless Commun.*, vol. 17, no. 7, pp. 4509–4521, Jul. 2018.
- [68] Y. Jeon, N. Lee, and H. V. Poor, "Robust data detection for MIMO systems with one-bit ADCs: A reinforcement learning approach," *IEEE Trans. Wireless Commun.*, vol. 19, no. 3, pp. 1663–1676, 2020.
- [69] J. Munir, D. Plabst, and J. A. Nossek, "Efficient equalization method for cyclic prefix-free coarsely quantized massive MIMO systems," in *Proc. IEEE Int. Conf. Commun.*, 2018, pp. 1–6.

- [70] M. Mohammadkarimi and M. Ardakani, "Optimal channel equalizer for mmwave massive MIMO using 1-bit adcs in frequency-selective channels," *IEEE Commun. Lett.*, vol. 24, no. 4, pp. 882–885, 2020.
- [71] M. K. Samimi, G. R. MacCartney, S. Sun, and T. S. Rappaport, "28 ghz millimeter-wave ultrawideband small-scale fading models in wireless channels," in *Proc. IEEE Veh. Technol. Conf.*, 2016, pp. 1–6.
- [72] Y. Jeon, H. Do, S. Hong, and N. Lee, "Soft-output detection methods for sparse millimeter-wave MIMO systems with low-precision ADCs," *IEEE Trans. Commun.*, vol. 67, no. 4, pp. 2822–2836, 2019.
- [73] G. M. Guvensen, Y. Tanik, and A. O. Yilmaz, "A reduced-state ungerboeck type MAP receiver with bidirectional decision feedback for m-ary quasi orthogonal signaling," *IEEE Trans. Commun.*, vol. 62, no. 2, pp. 552–566, Feb. 2014.
- [74] S. Jacobsson *et al.*, "Massive MU-MIMO-OFDM uplink with hardware impairments: Modeling and analysis," in *Proc. Asilomar Conf. Signals Syst Comput.*, 2018, pp. 1829–1835.
- [75] S. Jacobsson *et al.*, "Linear precoding with low-resolution DACs for massive MU-MIMO-OFDM downlink," *IEEE Trans. Wireless Commun.*, vol. 18, no. 3, pp. 1595–1609, Mar. 2019.
- [76] J. J. Bussgang, "Crosscorrelation functions of amplitude-distorted Gaussian signals," Res. Lab. Elec., Cambridge, MA, USA, Tech. Rep., Mar. 1952.
- [77] O. T. Demir and E. Björnson. (2020, May 4) *The Bussgang Decomposition of Non-Linear Systems: Basic Theory and MIMO Extensions*. [Online]. Available: <https://arxiv.org/pdf/2005.01597.pdf>
- [78] J. H. V. Vleck and D. Middleton, "The spectrum of clipped noise," *Proc. IEEE*, vol. 54, no. 1, pp. 2–19, 1966.
- [79] T. Brown *et al.*, *Practical guide to MIMO radio channel: With MATLAB examples*. Hoboken, NJ, USA: Wiley, 2012.
- [80] A. Mezghani and J. A. Nossek, "Capacity lower bound of MIMO channels with output quantization and correlated noise," in *Proc. IEEE Int. Symp. Inf. Theory*, Cambridge, MA, 2012.
- [81] O. Orhan *et al.*, "Low power analog-to-digital conversion in millimeter wave systems: Impact of resolution and bandwidth on performance," in *Proc. Inf. Theory and Appl. Workshop*, San Diego, CA, 2015, pp. 191–198.
- [82] A. Mezghani *et al.*, "A modified MMSE receiver for quantized MIMO systems," *Proc. ITG/IEEE WSA*, 2007.
- [83] G. Ungerboeck, "Adaptive maximum-likelihood receiver for carrier-modulated data-transmission systems," *IEEE Trans. Commun.*, vol. 22, no. 5, pp. 624–636, May. 1974.
- [84] G. Colavolpe, D. Fertonani, and A. Piemontese, "SISO detection over linear channels with linear complexity in the number of interferers," *IEEE J. Sel. Topics Signal Process.*, vol. 5, no. 8, pp. 1475–1485, Dec. 2011.
- [85] F. R. Kschischang, B. J. Frey, and H. . Loeliger, "Factor graphs and the sum-product algorithm," *IEEE Trans. Inf. Theory*, vol. 47, no. 2, pp. 498–519, Feb. 2001.
- [86] M. Ivanov, C. Hger, F. Brnstrm, A. Graell i Amat, A. Alvarado, and E. Agrell, "On the information loss of the max-log approximation in BICM systems," *IEEE Trans. Inf. Theory*, vol. 62, no. 6, pp. 3011–3025, Jun. 2016.
- [87] G. M. Guvensen, Y. Tanik, and A. O. Yilmaz, "A reduced-state ungerboeck type MAP receiver with bidirectional decision feedback for m-ary quasi orthogonal signaling," *IEEE Trans. Commun.*, vol. 62, no. 2, pp. 552–566, Feb. 2014.
- [88] G. M. Güvensen, "A reduced complexity Ungerboeck type receiver for multi-code signaling in dispersive channels," Ph.D. dissertation, MIDDLE EAST TECHNICAL UNIVERSITY, 2014.
- [89] P. Viswanath *et al.*, "Optimal sequences, power control, and user capacity of synchronous CDMA systems with linear MMSE multiuser receivers," *IEEE Trans. Inf. Theory*, vol. 45, no. 6, pp. 1968–1983, Sept. 1999.
- [90] A. Lapidoth, "Mismatched decoding and the multiple-access channel," *IEEE Trans. Inf. Theory*, vol. 42, no. 5, pp. 1439–1452, 1996.
- [91] M. Salehi and J. Proakis, *Digital Communications*. New York, NY, USA: McGraw-Hill, 2007.
- [92] U. H. Rizvi, G. J. M. Janssen, and J. H. Weber, "BER analysis of BPSK and QPSK constellations in the presence of ADC quantization noise," in *Proc. Asia-Pacific Conf. Commun.*, 2008, pp. 1–5.